AN ABSTRACT OF THE THESIS OF

Jill E. Magnusson for the degree of Master of Science in Nuclear Engineering presented on June 3, 2011

Title: Pressure Effects on Density-Difference Driven Stratified Flow: CFD Model of a DCC event in the HTGR

Abstract approved:

_____

Brian G. Woods

In a Modular High Temperature Gas Reactor (MHTGR), the Depressurized Conduction Cooldown (DCC) event can be separated into three distinct stages: 1) depressurization, 2) air ingress and, 3) natural circulation. During normal operations, the HTGR utilizes forced convection to move the helium coolant through the reactor core. Thus, during normal operations the helium is pressurized to about 7 MPa. As a result of the high pressure system, when a DCC event is initialized, there exists a pressure difference between the helium coolant inside the vessel and the ambient air outside the vessel. After depressurization there exist an air-helium mixture of higher density than the helium in the reactor vessel. This results in the air-helium mixture ingressing into the reactor vessel through stratified flow.

The High Temperature Test Facility (HTTF), under construction at Oregon State University, is a scaled model of the MHTGR. The HTTF is being built for code validation purposes. This study is to utilize CFD methods to simulate a DCC event in the HTTF. With this CFD simulation the effects of the depressurization stage on the rest of the model will be quantified.

Pressure Effects on Density-Difference Driven Stratified Flow: CFD Model of a DCC event in the HTGR

by

Jill E. Magnusson

A THESIS

submitted to

Oregon State University

in partial fulfillment of

the requirements for the

degree of

Master of Science

Presented June 3, 2011

Commencement June 2012

Master of Science thesis of Jill E. Magnusson presented on June 3, 2011.

APPROVED:

_____

Major Professor, representing Nuclear Engineering

_____

Head of the Department of Nuclear Engineering and Radiation Health Physics

_____

Dean of the Graduate School

I understand that my thesis will become part of the permanent collection of Oregon State University libraries. My signature below authorizes release of my thesis to any reader upon request.

_____

Jill E. Magnusson, Author

ACKNOWLEGEMENTS

I would sincerely like to express my appreciation to all the individuals without whose support I would not be where I am today. Firstly, I would like to thank my advisor, Dr. Brian Woods, who has provided me with direction and encouragement. His knowledgeable guidance has successfully led me through my time as a graduate student and has prepared me for a future in the nuclear field.

I would also like to thank my fellow graduate students who have often given of their time to listen, discuss, and reason through many of my academic problems. I would also like to express my gratitude to Seth Cadell and Brian Jackson and thank them for sharing their wealth of CFD knowledge with me.

I would like to thank all my family members who have supported me throughout this process. I feel an immense amount of gratitude to my parents, Steve and Carolyn Smith, for the love of learning they instilled in me as a child and for their endless encouragement throughout my lengthy academic career. Lastly, I would like to thank my loving husband, Lee Magnusson, who for the past two years has been a source of strength as I have struggled through many difficult trials.

TABLE OF CONTENTS

TABLE OF CONTENTS (Continued)

LIST OF TABLES

LIST OF FIGURES

Figure Page

LIST OF FIGURES (Continued)

Figure Page

NOMENCLATURE

SYMBOLS

F	densimetric Froud number
u	fluid velocity
h	enthalpy
$q_r^{"}$	heat flux
S	source term
Φ	dissipation
g	gravity
g'	reduced gravity
d	hydraulic depth
ρ	density
P	pressure
K	mean kinetic energy
U	mean velocity
μ	Viscosity
s_{ji}	linear deformation
k	kinetic energy
ε	energy dissipation

PRESSURE EFFECTS ON DENSITY-DIFFERENCE DRIVEN STRATIFIED FLOW: CFD MODEL OF A DCC EVENT IN THE HTGR

1 BACKGROUND

1.1 Problem Background

The modular high temperature gas reactor (MHTGR), as proposed by General Atomics, is a gas cooled, graphite moderated reactor. The MHTGR utilizes a prismatic core consisting of prismatic graphite blocks that act as the reactor's moderator. The core itself is annular featuring annular inner and outer graphite reflectors. TRISO coated fuel is embedded in the graphite and placed in the prismatic blocks. During normal operations the fuel is designed to operate at temperatures less than 1250 °C.

The gaseous helium coolant enters the core around 259 ° C through a concentric inlet-outlet duct. Forced convection then causes the gas to flow up through the upcomer, a space between the outer reflector and the inner vessel wall. This helps maintain the vessel wall temperature within allowable limits. The helium then exits the upcomer and enters the upper plenum. The gas is then forced downward through the upper core supports and pushed into the fuel elements and coolant channels of the prismatic blocks. Finally, the helium enters the lower plenum where it is the forced out the concentric inlet-outlet duct (see figure 1.1 for the basic concept of the MHTGR design). It is predicted that the average temperature rise across the core will be around 428 °C causing well

mixed coolant to exit the vessel around 687 °C. Due to the nature of forced convection the inside of the vessel is pressurized to 6.39 MPa.

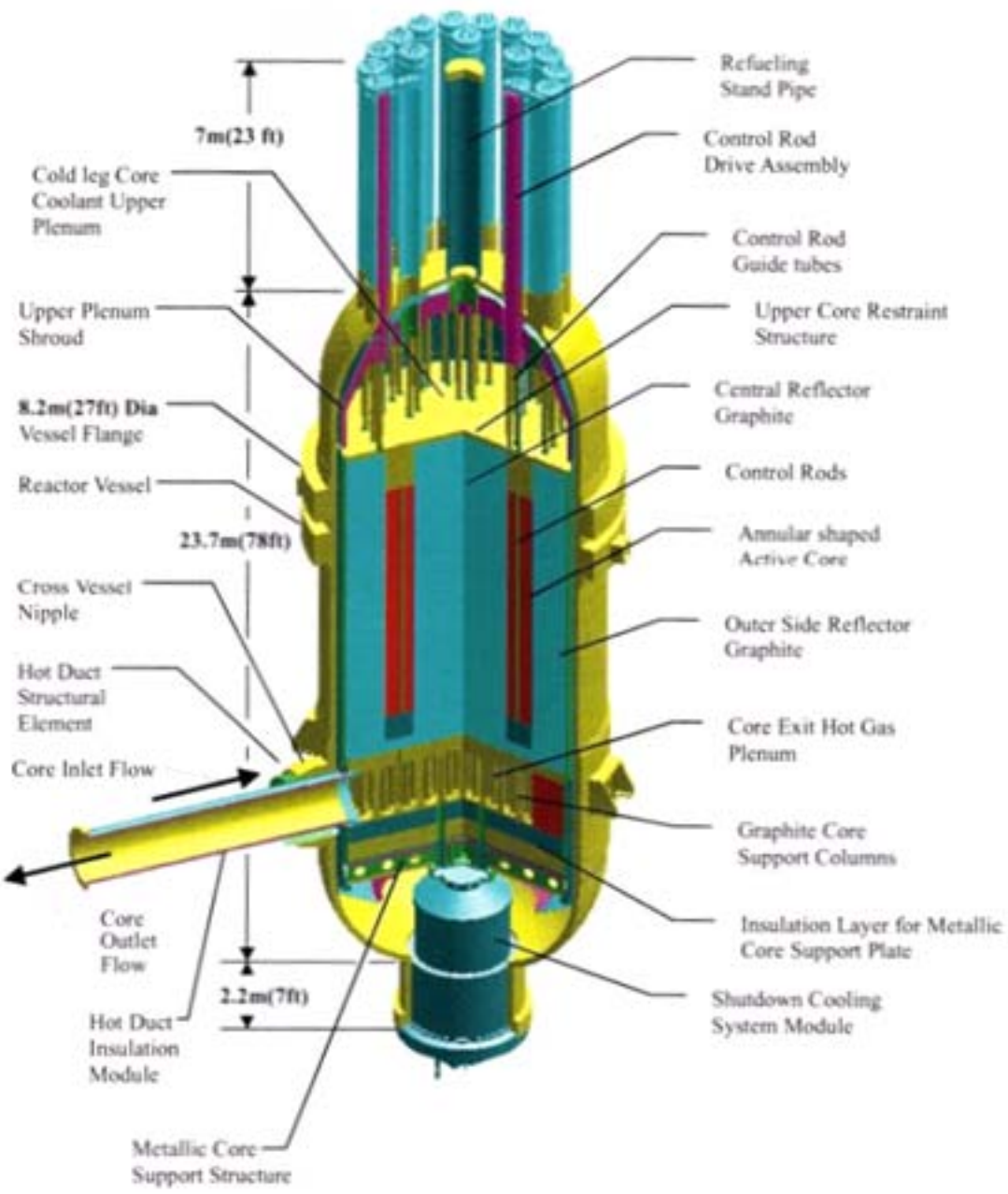

Fig 1.1: Image of the GT-MHR which is similar to the MHTGR [26].

Before an MHTGR can be built, extensive theoretical and experimental research on possible accident scenarios must be conducted. One such scenario would be the depressurized loss of forced convection with air ingress, D-LOFC, also known as a depressurization conduction cooldown event, DCC. The onset of a DCC is caused by a breach of the system's pressure boundary. In the event of a break along the inlet/outlet duct, helium will rush out into the air filled reactor cavity and the core will depressurize. The occurrence of depressurization provides the opportunity for a helium air mixture, occupying the reactor cavity, to ingress into the core. This may have a significant impact on the vessel as the oxygen in the air may oxidize the graphite which in turn may degrade internal structural integrity. There can be a wide range of depressurization rates, air ingress rates, and oxygen content in the reactor cavity depending upon size and location of the break as well as design specific considerations.

A worst case scenario DCC would be in the instance of a double ended guillotine break, where the break would involve a complete cut through the inlet/outlet duct. In this case after depressurization has occurred, there would exist a helium air mixture in the reactor cavity. Due to the large temperature difference and gas concentrations between the reactor cavity and the vessel, the He-air mixture is always denser than the helium contained in the vessel. It is this density difference that allows for the preliminary stages of air ingress to begin by inducing a gravity driven stratified flow also known as exchange flow (see figure 1.2). In exchange flow, the denser fluid flows along the bottom of the inlet/outlet duct and empties into the lower plenum of the reactor vessel.

This allows for less dense fluid to flow out along the top of the duct. This flow continues until helium-air mixture reaches a thermally stratified state where the mixture can no longer flow into the vessel. It is at this point that air ingress continues through molecular diffusion(see figure 1.3). During molecular diffusion, air molecules diffuse upward into the existing helium molecules while helium molecules diffuse downward into the helium-air mixture. After the molecular diffusion stage, a distribution of gas temperature and concentration in the flow passages of the reactor induce a natural convection flow.

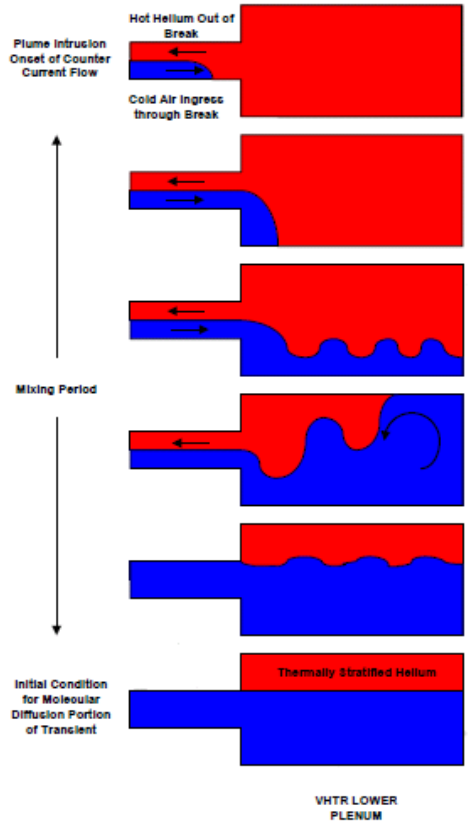

Fig 1.2: The initiation and development of exchange flow between a cooler, denser fluid (blue) and a hotter, less dense fluid (red).

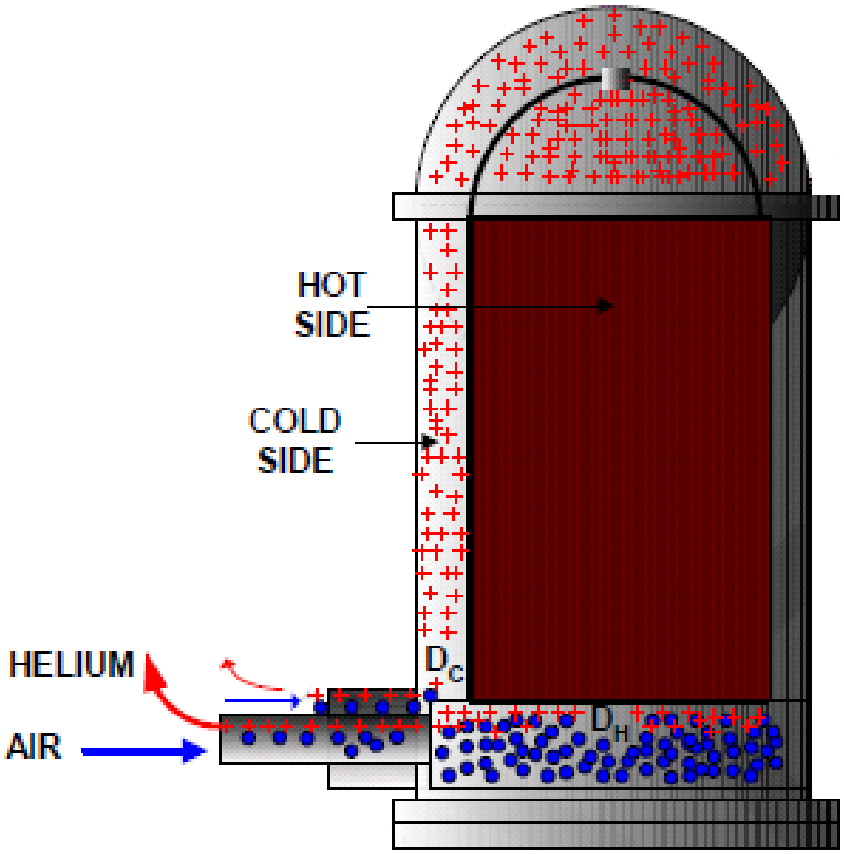

Fig 1.3: Depiction of molecular diffusion in gas reactor.

The high temperature test facility (HTTF), being constructed at Oregon State University, is a scaled facility designed to model the MHTGR and is to play an integral role in the licensing of MHTGR. This facility will be used to model the thermal hydraulics of design basis and beyond design basis scenarios, thus providing experimental thermal hydraulic data to validate computational thermal hydraulic codes. Specifically, the HTTF will provide data for the depressurized conduction cooldown event with the possibility of some data collection for a pressurized conduction cooldown

event (PCC). The HTTF has been designed to meet certain experimental objectives during each phase of a DCC transient, they are: the lower plenum temperature profiles during exchange flow air-ingress, the effects of the lower plenum structures on exchange flow phenomena, the rate of air-ingress by molecular diffusion, the time to onset of air natural circulation, the radial heat conduction temperature profiles, estimation of the thermal radiation heat transfer rates, the high temperature loop natural circulation flow rates following the air-ingress phase, and the effect of flow bypass flow areas on the transient behavior.

It was attempted to preserve the geometry of the MHTGR as part of the design of the HTTF (see figure 1.4). The HTTF is 1:4 scale in height and diameter. The HTTF also features a 1:8 pressure scale to the MHTGR along with a 1:1 temperature scale. Below table 1.1 provides the scaling ratios between the HTTF and the MHTGR.

Table 1.1: Scaling parameters between the HTTF and MHTGR.

Parameter	Scaled Ratio
Pressure	1 : 8
Temperature	1 : 1
Length	1 : 4
Diameter	1 : 4

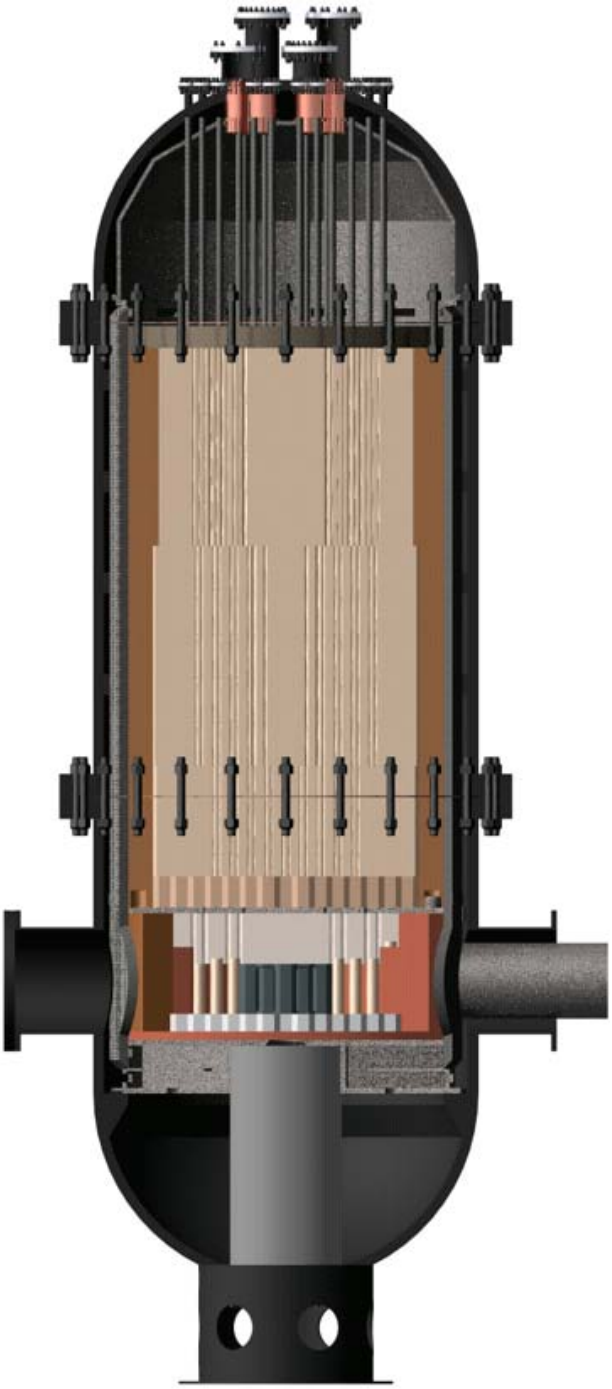

Fig 1.4: Depicts the geometry of the high temperature test facility. Notice the concentric inlet-outlet duct located on the right of the vessel in this picture. The duct on the left portion of the vessel is primarily for visualization studies in the HTTF and internal facility access.

1.2 Purpose

The occurrence of a depressurized conduction cooldown event poses several problems to a MHTGR. Of the utmost importance is air ingressing into the reactor vessel and oxygen reacting with the heated graphite. Due to the potential damage to the reactor's structural integrity, it is important to study the DCC event and the rate at which that event occurs. There are already several existing studies that investigate the molecular diffusion and exchange flow stages of the DCC event; however, there remains a gap in the understanding of the event's depressurization stage. When a break occurs along the pressure barrier, the internal pressure of the vessel creates a momentum driven flow that allows for the release of the coolant helium and results in the depressurization of the system. It is expected that pressure equilibrium between the inside and outside of the reactor will be reached in a very short time. It is only after a complete system depressurization that exchange flow occurs. However, due to the initial momentum behind the depressurization, it is possible that the exchange flow may not initiate as anticipated.

1.3 Objectives

As previously mentioned, there is a need to study the initial onset of the DCC event. The phenomena under investigation during the DCC event include the momentum driven depressurizing flow after the initial break occurs, followed by exchange flow, and molecular diffusion. It is these phenomena that are responsible for the concentration of air ingress and the time scale in which the accident occurs. It is the goal and focus of this

study to examine the effects that depressurization has on the initiation of exchange flow, the amount of air ingressed into the vessel through that process, and the time at which these phenomena take place.

1.4 Limitations and Assumptions

Due to computational limitations, a simplified geometry of the HTTF was utilized. These simplifications impose some limitations on the applicability to a true HTTF geometry and MHTGR geometry. Even though the simulated geometry may not be directly applicable to the true geometries, it is reasonable to expect similar behavior despite slight changes in the geometry.

2 LITERATURE REVIEW

The purpose of this chapter is to outline previous studies conducted pertaining to the DCC event, stratified flow, and molecular diffusion.

2.1 Air Ingress

Initial studies into the DCC event began by researching methods of air ingress into the reactor vessel. It was initially believed that the only significant amount of air would enter the reactor vessel from molecular diffusions. Therefore early DDC studies deal primarily with molecular diffusion. Later it was hypothesized that a significant amount of air may enter the reactor vessel through lock exchange flow causing natural circulations to initiate much sooner than was earlier anticipated. Subsequent DCC studies focused on air ingress through lock exchange flow. This section is to outline those studies dealing with air ingress through molecular diffusion and lock exchange flow.

2.2 Molecular Diffusion

The different stages of the depressurized conduction cooldown event are understood at various levels. The earlier studies of a DDC event in a high temperature gas reactor indicated that the dominate cause of air ingress comes only from molecular diffusion [1,2,3,4,5]. Air ingress by diffusion was primarily studied by two groups; the Japanese Atomic Energy Research Institute (JAERI), and the Jülich Research Center, in Germany. At JAERI, both analytical and experimental methods were used to gain an

understanding of how the phenomena of diffusion, and natural circulation effects air ingress [1,2,3,4].

The high temperature engineering test reactor (HTTR) was developed at JAERI as a high temperature, graphite moderated, gas cooled thermal reactor. It features a similar design to the HTGR with the exception of a concentric vertically standing inlet/outlet duct. It is assumed that a coaxial-tube rupture is the most severe design basis accident for the HTTR (see 5ure 4). Similarly, to the MHTGR , a DCC event in the HTTR is the result of a rupture on the main pipe and the high pressured helium is blown out of the reactor. However, the reactor's depressurization is expected to be complete within a few minutes. In this case, the heavier He-air mixture is below the less dense He in the reactor. This creates a stable gas layer and exchange between the two gases is delayed. Air is then transported into the reactor via molecular diffusion. This leads to a chemical reaction between O_2 and the graphite structure that produces a mixture comprising of He, N_2, O_2, CO, and CO_2. Natural convection is initiated by the distribution of gas temperatures in the reactor's flow passages.

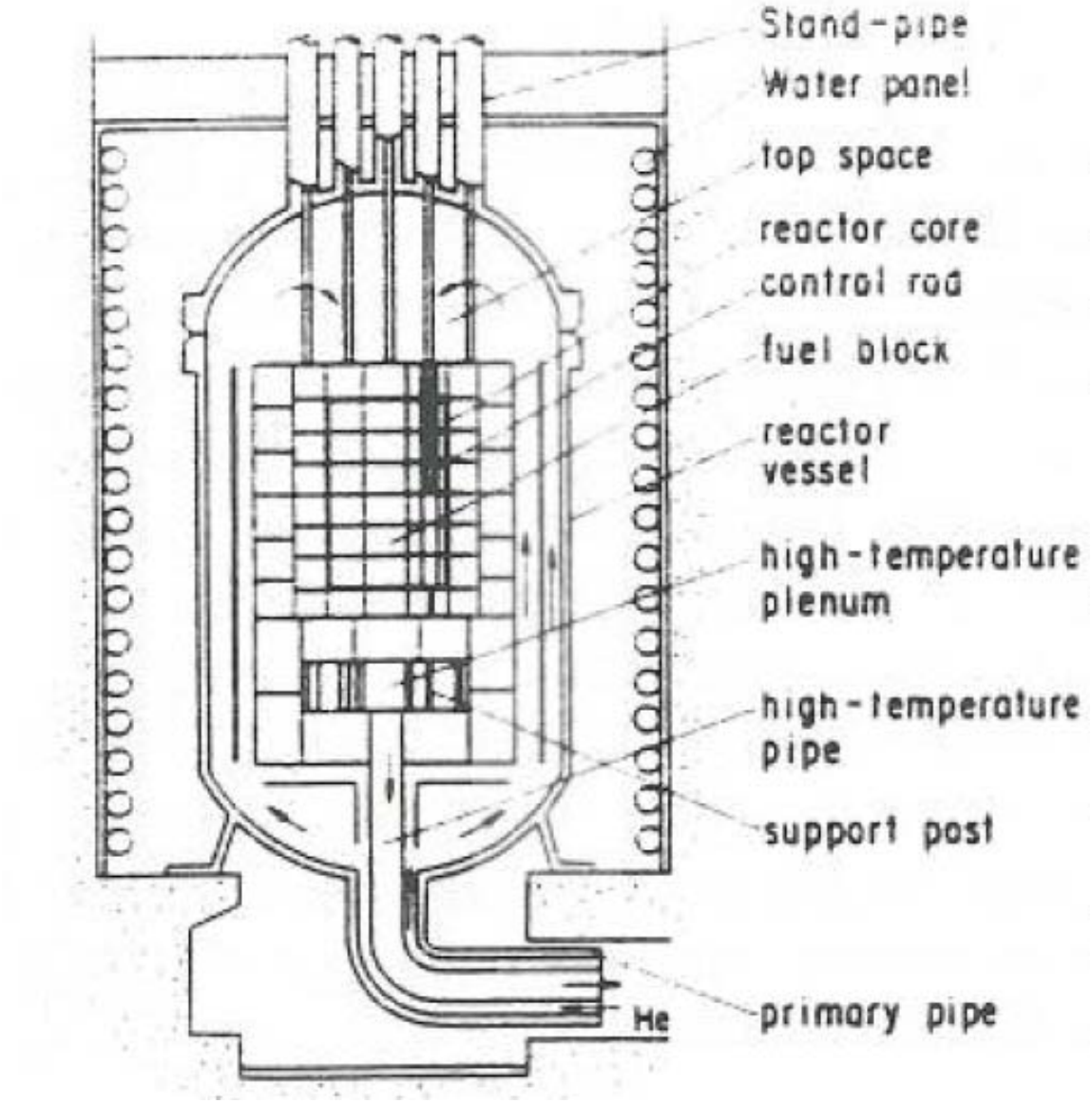

Fig 2.1: Is a schematic diagram of the HTTR developed at JAERI [3].

An analytical study of molecular diffusion and natural convection was conducted by Hishida and Takeda. For these calculations, a U shaped tube at equilibrium pressure

was used. It was assumed that the O_2 and graphite reaction would effect molecular diffusion so for this study air was assumed to be only N_2.

The analytical results indicated that the N_2 mole fraction increases very gradually with time. It also shows that the N_2 only enters the inverted U shaped tube through molecular diffusion and natural convection stimulated by buoyancy forces that are created from the gas temperature distributions and that natural circulation is not initiated until 30 to 80 hours after the initial break. Hishida and Takeda also preformed an experimental test in an inverted U shaped tube to monitor the molecular diffusion and natural circulation phenomena. They found that the experimental values agreed well with the obtained analytical values [4].

Hishida et al. conducted further experimental tests to compare the air ingress with and without the air-graphite reaction. The test rig contained a graphite high temperature plenum and a reactor core simulator. Inside the simulator were seven graphite tubes. The first experiment used air and helium as the working fluids. The second experiment N_2 and He were used as the fluids to demonstrate diffusion without the O_2 graphite reaction. In both tests, the density changes in the plenum were monitored and the time to natural circulation was recorded. The test results indicated that the density change was almost the same for both experiments. For both, the density increased slowly as time elapsed with a sharp increase just before the onset of natural circulation. Also, both tests indicated a similar onset time for natural circulation [3].

The JAERI experimental tests were benchmarked by Kadak and Zhai using computational fluid dynamic analysis. For their benchmarking project, FLUENT-6 was used as the CFD code. It was chosen for various reasons, but primarily for its abilities to compute multicomponent chemical reactions. For the initial JAERI experiment, the working fluids were defined as He and N_2. FLUENT produced results that were in good agreement with the experimental values obtained by Hishida and Takeda, demonstrating that CFD methods (specifically FLUENT) can be used to model molecular diffusion without chemical reactions during a depressurized conduction cooldown event [1].

Jülich Research Center, in Germany, Wolters et al. experimentally investigated gas exchange through a failed tube after depressurization. In this experiment, a long vertical tube connects a helium filled container to the environment. This geometry assumes that air ingress results primarily from molecular diffusion. By using the obtained experimental velocities the air ingress into the system may be simply estimated. According to the results of this experiment the quantity of air entering the primary circuit is minimal, so small that the O_2-graphite reaction and graphite corrosion is negligible. It is estimated that in the very worst case scenario a minimum of 19 hours would elapse before corrosion induced fission products would be released [2].

2.3 Exchange Flow

Initial studies assume that the majority of air ingress is caused primarily by diffusion. Subsequent studies have shown that this is not the case. Rather, a significant amount of air ingress occurs due to lock exchange flow that is initiated after the system's depressurization [6,7,8,9,10,11,12]. The worst case scenario for a HTGR or VHTR is hypothesized to be a double ended guillotine break along the concentric inlet/outlet duct. This would result in a large break LOCA and the initiation of a DCC event. Oh *et. al*. made preliminary lock exchange flow calculations using FLUENT. A simplified core version of the GT-MHR 600MWt was used for the simulation's basic geometry and the pressure was uniformly set equal to 1 atm. As part of the simplification, the core was modeled as a porous material. From this CFD study, it was observed that following depressurization air ingresses into the reactor vessel via stratified exchange flow at a much quicker time scale than previously observed during air ingress through molecular diffusion [9].

In effect, stratified flow is based on the assumption that the air makes a wedge formation in the lower half of the duct that advances into the reactor as a function of density gradient [10]. This flow can be characterized by the densimetric Froude number, F

$$F = \frac{u}{\sqrt{g'd}} \tag{1}$$

Where u is the discharge air velocity, d is the hydraulic air depth and g' is reduced gravity.

$$g' = \frac{g\left(\rho_2 - \rho_1\right)}{\frac{\rho_2 + \rho_1}{2}} \tag{2}$$

F indicates the magnitude of inertial forces relative to the buoyancy force created due to stratification. In this CFD simulation, the GAMMA code was used and it was found that air filled the lower plenum very rapidly. Natural convection was initiated roughly 2 to 3 minutes after the beginning of exchange flow. This is a considerably faster time scale than what was predicted with diffusion being the primary means of air ingress. Due to uncertainty pertaining to the flow regimes upon air ingress initiation this study also takes into account four different flow regimes during isothermal conditions. It was found that the laminar model is the most conservative due to the fact that there is no mixing dissipation and thus predicts the largest amount of air ingress into the reactor vessel. In the other turbulent models a mixing term lessens the effects of the density gradient, the flow's driving force [10].

Duncan and Toor conducted a two bulb experiment where two bulbs of 77.99 cm^3 and 78.63 cm^3 volume are connected by a capillary tube 8.59 cm long and a 2.08 cm diameter. Each bulb was filled with a gas. Different combinations of N_2, H_2, and CO_2 were used for the two component gas flow [15]. Oh preformed a CFX simulation for Duncan and Toor's two bulb experiment. The results of his study agreed well with those

experimentally obtained by Duncan and Toor. Oh's study also indicated that the size of the horizontal pipe effects whether diffusion or stratified flow is the predominate source of gas movement. According to Oh's CFX study in a 2 mm horizontal tube, molecular diffusion was the dominant phenomenon for gas flow; while in a 16 mm tube, the gas flow was dominated by density gradient stratified flow [10].

Oh also conducted other CFD and CFX studies providing code validation for stratified flow. This study used experimental data collected by ETH Zurich and was conducted using FLUENT for gases of density ratios ranging from 0.046 to 0.90. He found that the CFD predicted axial velocities agreed very well with those obtained experimentally [14]. Later studies conducted by Oh indicated natural circulation may occur much faster than previously predicted [11]. Calculations performed by Oh indicated a time of 19.5 s for air in stratified flow to reach the center of the lower plenum while a time for molecular diffusion was found to be 1.29×10^4 s [12]. The significant difference between the two initiation times shows the importance of the dominating exchange flow phenomenon during air ingress.

The above studies deal with the behavior in a HTGR during a DCC and it has been shown that the predominant method of air ingress into the reactor core during such an accident is due to lock exchange flow. However, none of these studies investigate the effects caused by the accident's initial depressurization. During depressurization an initial momentum is created. This momentum may cause a verity of phenomena before lock exchange flow can initiate.

3 CFD MODEL

CFD solvers, such as STAR-CCM+, uses a series of basic equations to make their calculations. These equations, in one dimension, are the conservation of mass also known as the continuity equation

$$\frac{\partial \rho}{\partial t} + \frac{\partial}{\partial x}\partial\left(\rho \mu_x\right) = 0 \tag{3}$$

the conservation of momentum equation

$$\frac{\partial}{\partial t}\left(\rho u_x\right) + \frac{\partial}{\partial x}\left(\rho u_x^2\right) = \frac{\partial p}{\partial x} + \mu \frac{\partial^2 u_x}{\partial x^2} + \rho g_x \tag{4}$$

and the conservation of energy

$$\frac{\partial}{\partial t}\left(\rho h\right) + \frac{\partial}{\partial x}\left(\rho u_x h\right) = \frac{\partial p}{\partial t} + u_x \frac{\partial p}{\partial x} + k \frac{\partial^2 T}{\partial x^2} + q_r^{"} + \Phi + S \tag{5}$$

and the equations of state

$$\begin{aligned} p &= p\left(\rho, t\right) \\ h &= h\left(\rho, t\right) \end{aligned} \tag{6}$$

This chapter outlines the methods used to construct the CFD models utilized in this study. It presents the three initial conditions cases used and the geometry that was applied to them. It also describes the meshing methods and physics used.

3.1 Geometry

The utilized geometry was created to simulate an early design of the high temperature test facility. This design consisted of two cylindrical tanks with hemispheric

ends connected by a long cross duct. The larger of the two tanks is to simulate the reactor core and would be heated in the HTTF. The smaller tank acts as what will from here on out be referred to as a blow down tank. This blow down tank will be filled with air at atmospheric pressure but is used to simulate the reactor cavity surrounding the vessel.

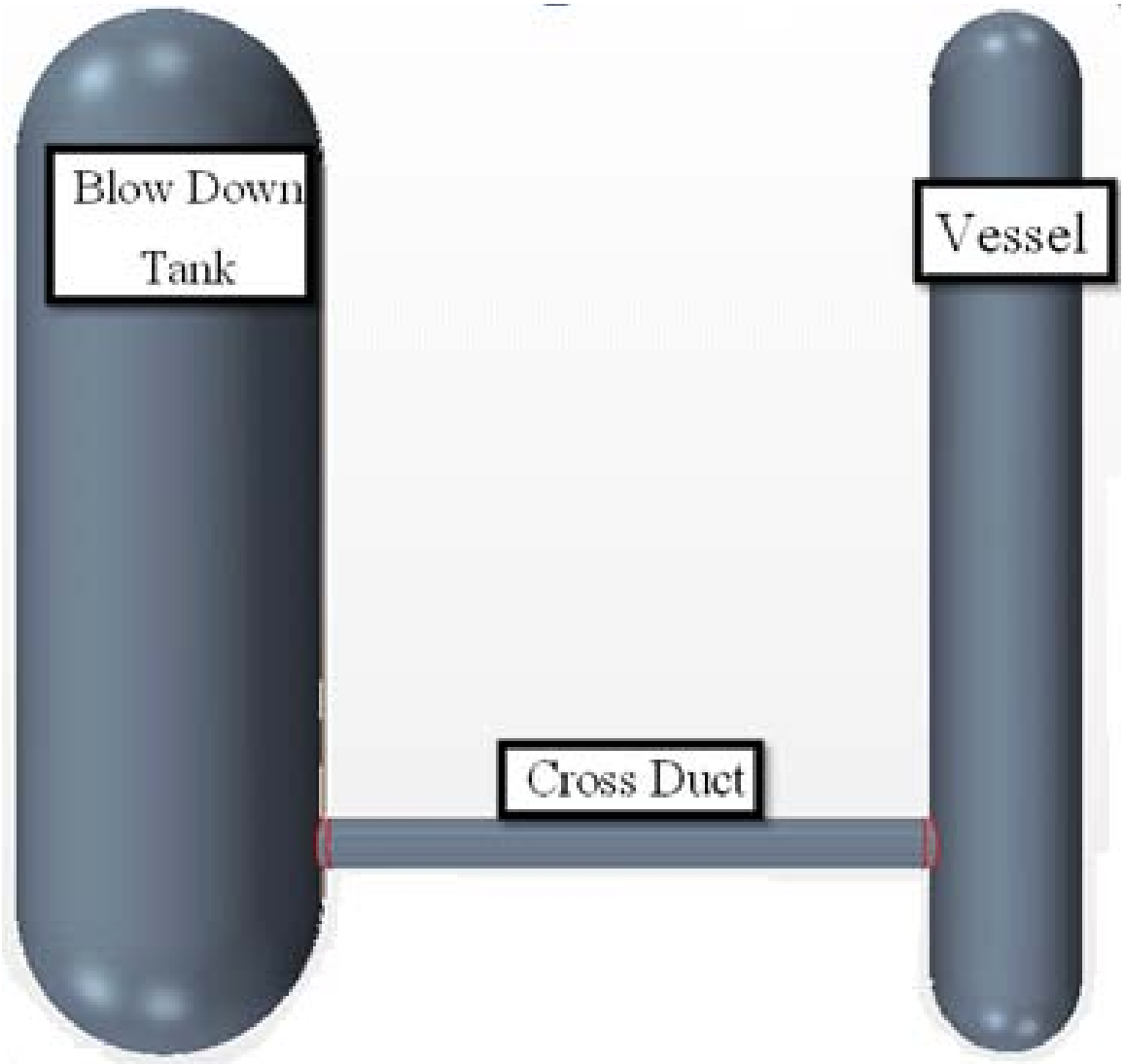

Fig 3.1: Geometry used for the CFD simulation. On the left is the air filled blow down tank and on the right is the helium filled and heated reactor vessel. As can be seen, the two are joined by a long horizontal cross duct.

In this model the blow down tank is 14.4115 m^3, the vessel is 3.8030 m^3 and the cross duct is 0.2714 m^3. As can be seen from figure 3.1, this geometry is greatly simplified from those seen in figures 1.1 and 1.4. In other CFD simulations, the internal components of the vessel have been modeled as porous materials [9]. These models were mostly used in studies to observe molecular diffusion and the onset of natural circulation. As this study focuses primarily on flows exiting and entering the vessel opposed to the flow moving inside the vessel, such as diffusion and natural circulation, a simplified geometry of the HTTF core is sufficient and desirable as it decreases computational time.

3.2 Initial Conditions

In this study three different sets of initial conditions were utilized. The first set of initial conditions was selected to provide a basic understanding of the system's behavior. The whole system was set to an equal pressure of 1 atm. The temperature in the vessel was set to the operating temperature of MHTGR, 670 °C, and the blow down tank was assumed to be at room temperature, 22 °C. The vessel was assumed to be filled with 100% helium and the blow down tank was entirely filled with air.

The second simulation, case 2, begins with the vessel pressurized to 0.8 MPa, and heated to 670 °C, which are the operating conditions of the HTTF. The blow down tank is assumed to be at atmospheric pressure, 1 atm, and room temperature, 22 °C. In this case the vessel was once again completely filled with helium and the blow down tank

was completely filled with air. These initial conditions were selected to observe the effects that momentum caused by depressurization would have on the subsequent air ingress.

The initial conditions of the 3rd case were determined upon the basis of investigating a DCC event with the assumption that the HTTF system had already undergone depressurization; however, the correct initial conditions for temperature, pressure and molecular composition in each tank are known. To do this the data from initial conditions case 2 was assessed and the temperature, pressure and molecular composition after the system's depressurization had completed was selected for the initial conditions of case 3. By using the data from case 2 to develop the initial condition for case 3, a direct comparison of how the initial momentum driven flow effects the molecular concentration in the vessel and the event's timing can be obtained. In this case the entire system was set to a constant pressure of 0.282697 MPa. The vessel and blow down tank were set to 634.3 °C and 118 °C respectively. Assuming this case is initiated immediately after depressurization, the vessel is still 100% helium while the blow down tank is composed of about 85% air and 15% helium. It can be assumed the gas components in the blow down tank are well mixed.

Table 3.1: The test matrix of initial conditions for the three different simulations run during this study.

Case	Air Press (Mpa)	Air Temp (C)	He Press (Mpa)	He Temp (C)	Vessel He %	Blow Down Tank He %
1	0.101325	22	0.101325	670	100	0
2	0.101325	22	0.8	670	100	0
3	0.282697	118	0.282697	634.3	100	15

3.3 Mesh

One of the first steps in the construction of a CFD model is building and refining the mesh or grid. The mesh subdivides the geometry into a number of smaller cells and information is passed from one cell to the next. Hence the mesh is what provides the special descritization for the model. To establish confidence in the solution obtained from the CFD model, it is essential that the solution be grid independent, or that it produce a solution that does not depend on the size or number of mesh cells present. To do this, the number of mesh cells is systematically increased to a point where the solution no longer changes after an increase in cell numbers. In this section, the meshing methods applied to the CFD model is described. It also describes the grid refinement processes and the results and conclusions of that process.

3.3.1 Mesh Type

For this study a polyhedral mesh was selected due to its relatively simple generation and efficiency. In a polyhedral mesh, arbitrary polyhedral cell shapes are put together to create the general mesh shape. In STAR-CCM+ specifically, a dual scheme

utilizes an inherent underlying tetrahedral mesh to create the polyhedral mesh. This also allows for the polyhedral mesh, on average, to contain five times fewer cells than the tetrahedral mesh, ultimately resulting in a faster computing time.

The polyhedral mesh can also be used with the generalized cylinder mesher, which is a mesh feature specifically designed for cylindrically shaped geometries. The generalized cylinder mesher creates orthogonal cells along the length of cylindrical areas. This results in a lower overall cell count and can enhance the rate of convergence. The generalized cylinder mesh is ideal for flows which move parallel to a geometry wall. This type of mesh is therefore ideal for this study where flow is moving parallel to a cylindrical cross duct.

3.3.2 Mesh Refinement

The initial model created to simulate the DCC event used only a polyhedral mesh without the generalized cylinder mesher. This was a relatively coarse mesh containing only 14,311 nodes. The geometry for this initial model was input as a single region causing the applied mesh to be a consistent size throughout. The geometry of the second model was input as three separate regions. These three regions were the vessel, blow down tank, and the cross duct. By inputting the geometry as three regions, one is able to apply finer meshes to areas of greater interest, such as the cross duct (see figures 3.1 and 3.2). The generalized cylinder mesher was also applied. The second model was the finest model that was run and featured a total of 66,433 nodes. 17,231 of those nodes were contained in the vessel, 31,527 nodes were in the blow down tank and 17,675 were

contained in the cross duct. A coarser mesh was then run utilizing the three region geometry input method and the generalized cylinder mesher. This mesh was made up of a total of 28,380 nodes with 16,213 in the vessel, 8,276 nodes in the blow down tank and 3,891 nodes contained in the cross duct. For the comparison of the three different mesh models, initial condition cases 1 and 2 were run with each mesh. Initial condition case 2 was selected as it was the only model simulating the depressurization stage, thus making it the most complex model. Initial condition case 1 was selected to observe the effects the mesh refinement had on the exchange flow stage.

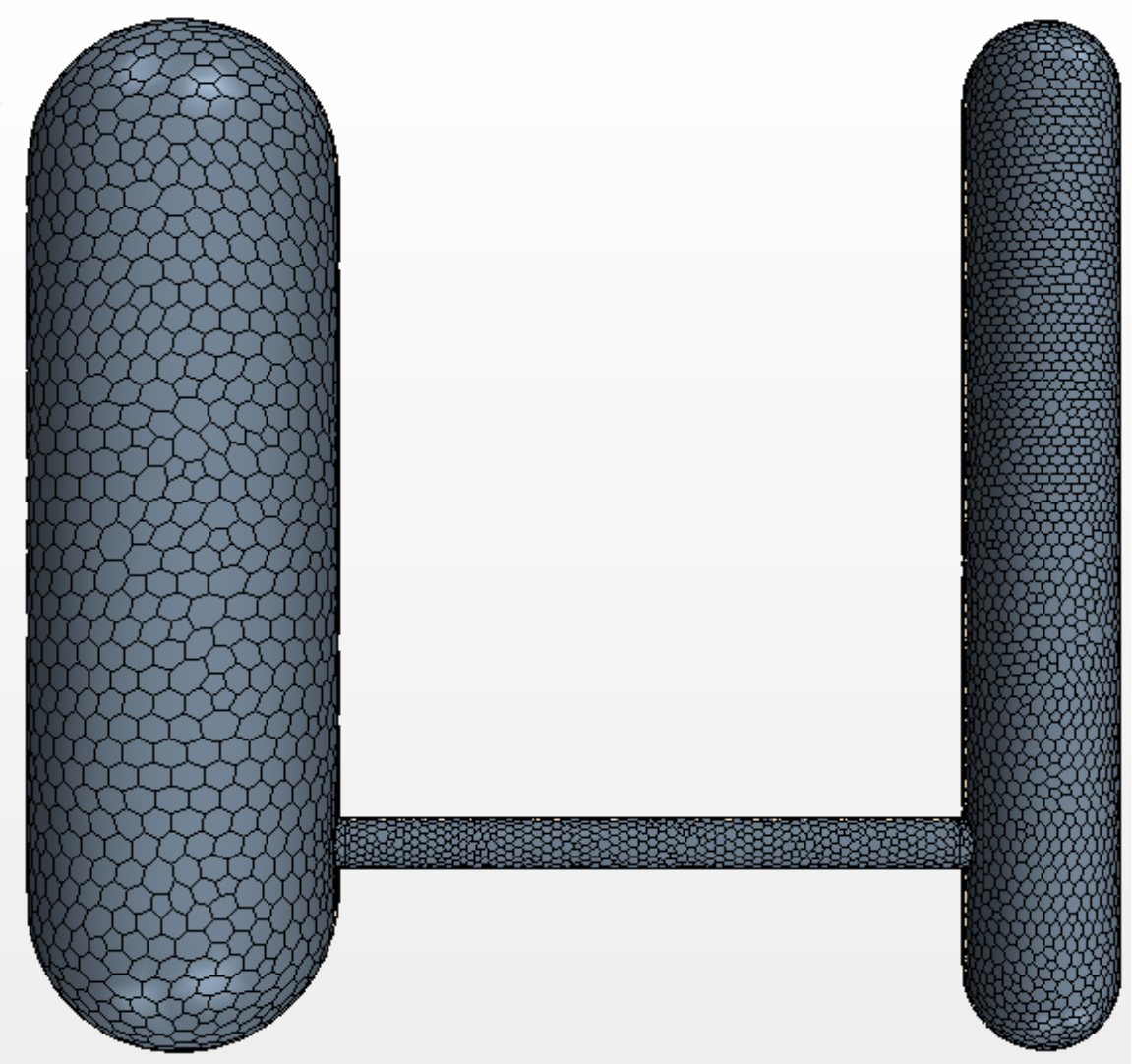

Fig 3.2: Depicts a mesh of mid-range coarseness with a total 28,380 nodes. This mesh also features a significantly finer mesh along the cross duct region.

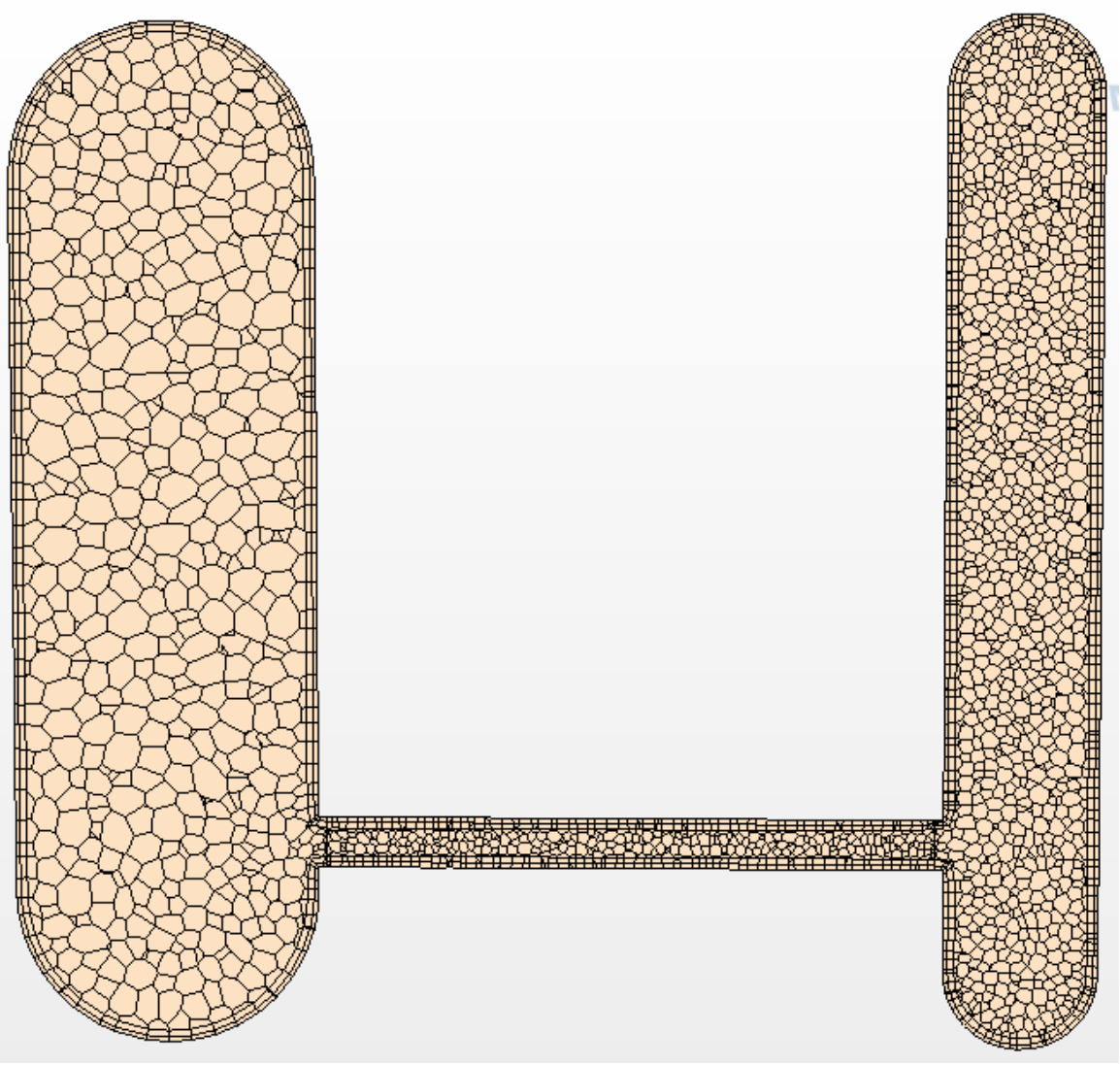

Fig 3.3: A view of the internal mesh scheme.

Table 3.2: Provides the three regions of the simulations geometry along with three different mesh models. The corresponding number of cells for each region is giving along with the total number of cells for the mesh model.

Mesh Model	# of Cells Blow Down Tank	# of Cells Cross Duct	# of Cells Vessel	Total # of Cells
Coarse	N/A	N/A	N/A	14311
Mid	8276	3891	16213	28380
Fine	31527	17675	17231	66433

Two figures of merit were used to examine convergence between mesh models. The first was temperature averaged over both the blow down tank and the vessel volumes. The second was the molecular composition as a percentage of helium present averaged over both the blow down tank and vessel volumes. These values were monitored due to their importance during a DCC event as they are two factors that may cause internal core damage. By monitoring these two factors, a better understanding of how the temperature reacts during a DCC event can be gained as well as a knowledge of the amount of air that actually ingresses into the vessel.

3.3.2.1 Vessel Mesh Refinement Data

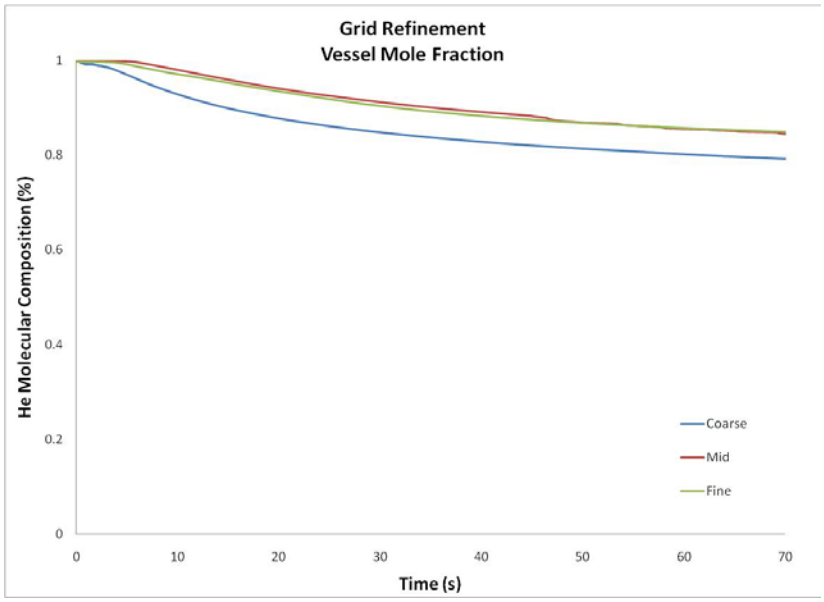

Fig 3.4: Provides the convergence monitor for initial condition case 2 where the molecular fraction as a percentage of helium present in the vessel versus time is monitored for three different mesh models.

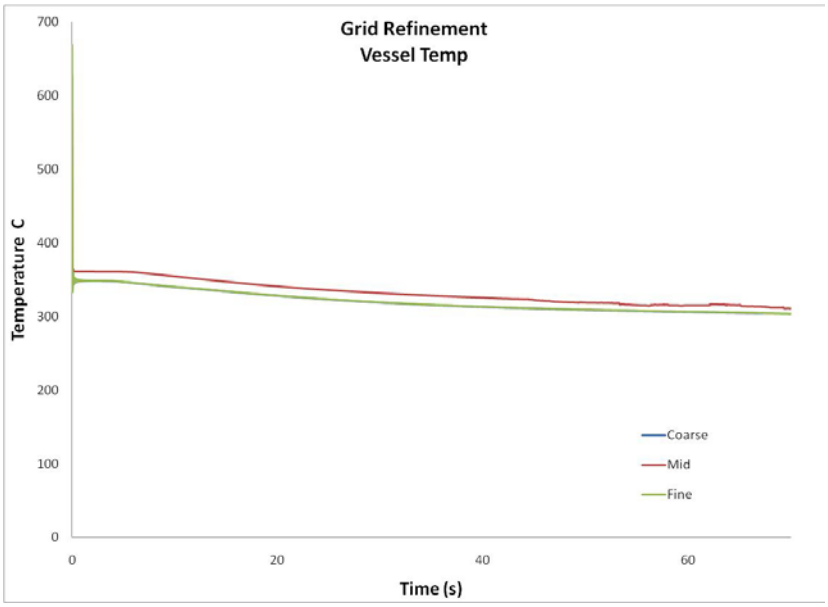

Fig 3.5: Provides the temperature convergence monitor, in the vessel for initial condition case 2, where the temperature versus time was monitored for 3 different mesh models.

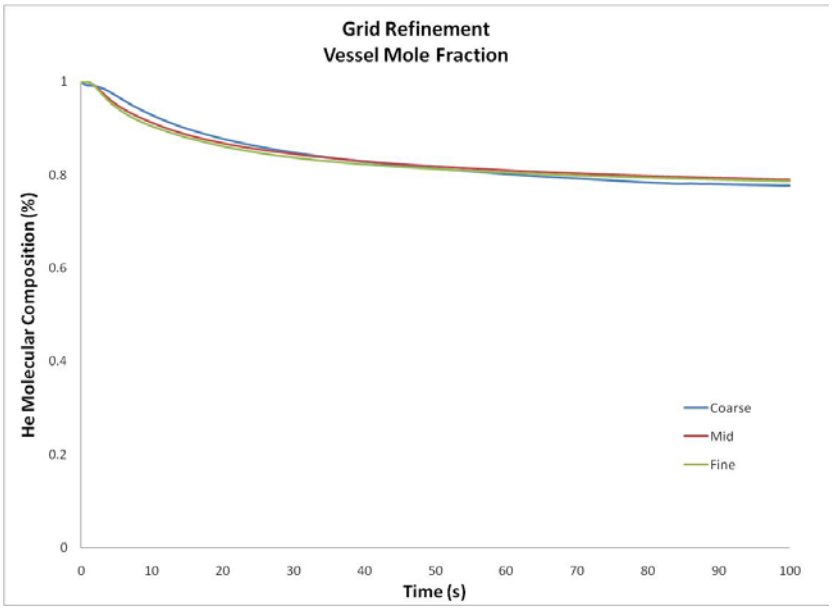

Fig 3.6: Provides the helium molecular composition monitor, in the vessel for initial condition case 1, where the average molecular fraction versus time is monitored.

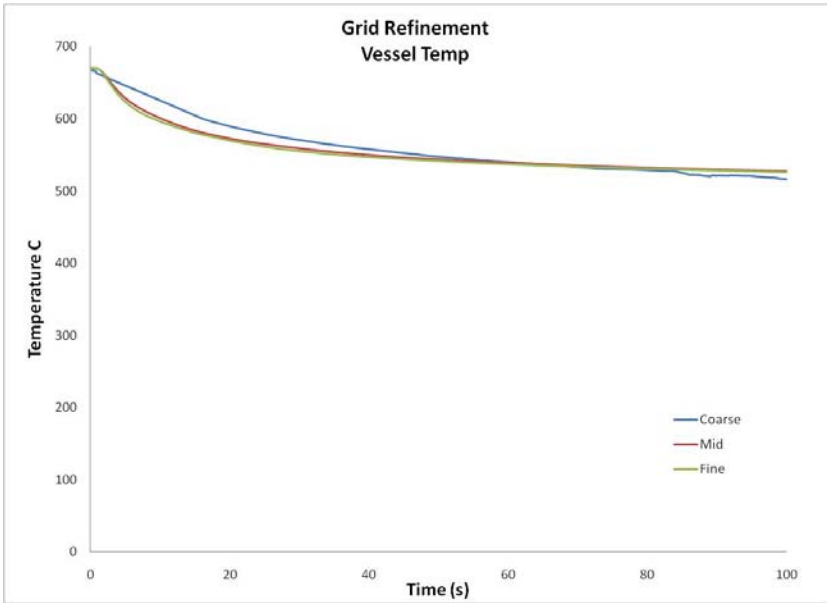

Fig 3.7: Provides the convergence monitor, in the vessel for initial condition case 1, where the average temperature versus time was monitored.

3.3.2.2 Blow Down Tank Mesh Refinement Data

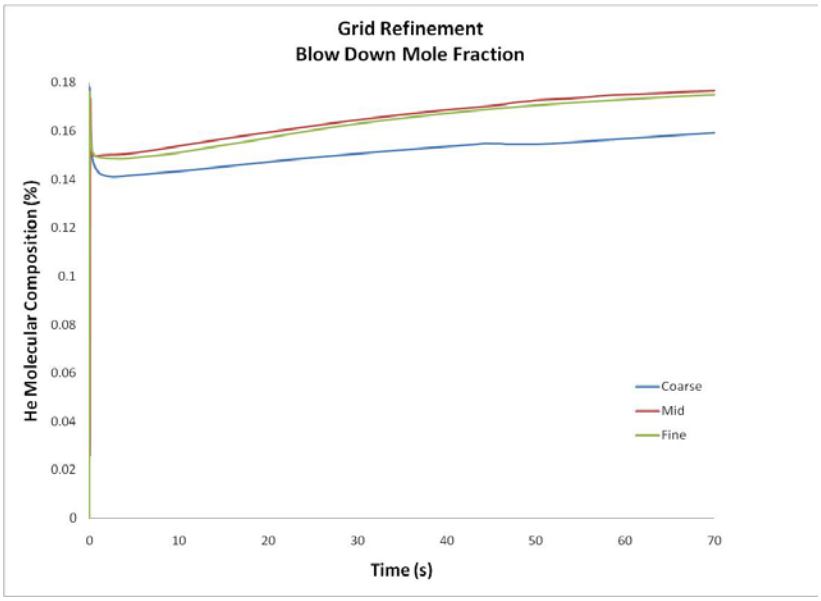

Fig 3.8: Provides the convergence monitor, in the blow down tank for initial condition case 2 where the helium molecular composition versus time is monitored.

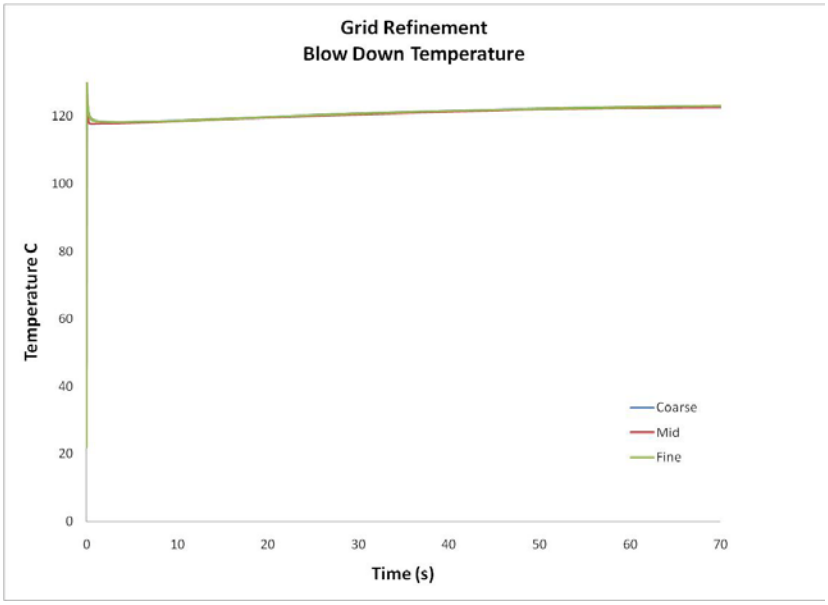

Fig 3.9: Provides the convergence monitor, in the blow down tank for initial condition case 2, where the temperature versus time was monitored.

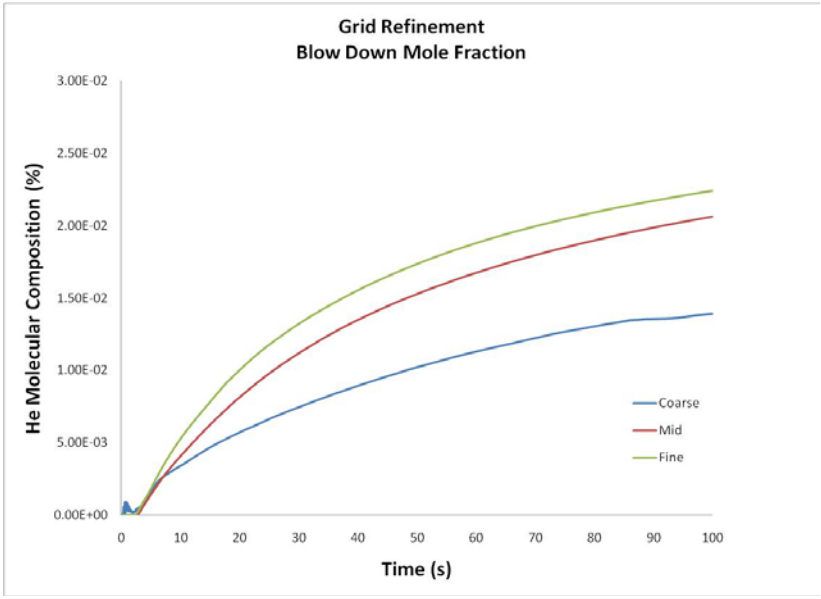

Fig 3.10: Provides the convergence monitor, in the blow down tank for the initial condition case 1, where the helium molecular composition versus time is monitored.

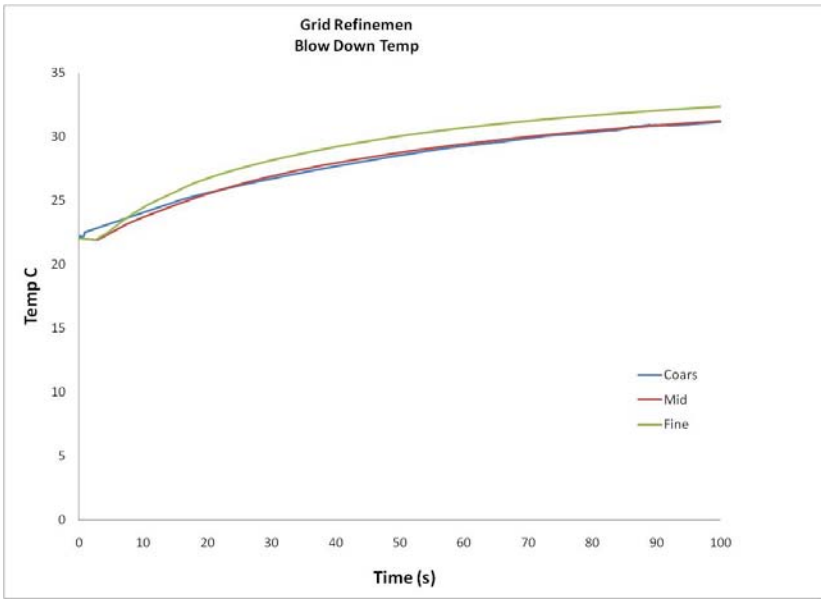

Fig 3.11: Provides the convergence monitor, in the blow down tank for initial condition case 1, where the temperature versus time is monitored.

3.3.2.3 Grid Refinement Conclusions

As can be seen from figures 3.4 through 3.11 above, that in most cases the data provided from the mesh with 28,380 nodes is very close to that provided from the mesh with 66,433 nodes. Calculating the difference from one mesh to another as

$$difference = \frac{|f_2 - f_1|}{f_1} \tag{7}$$

The difference averaged over time of the molecular composition in initial condition case 2 from the coarse to the mid mesh in the vessel was found to be roughly 0.061 while the average error from the mid to the fine mesh was only 0.0053. The temperature difference averaged over time was found to be slightly larger at 0.033 between both the coarse to mid and then mid to fine meshes. However, since the primary concern of this study is the amount of air ingressed into the vessel, it was determined that no further grid refinement was needed as the 28,380 node mesh accurately converges. In figures 3.4 and 3.10, the temperature data indicates that the coarse mesh (14,311 nodes) is more similar to the fine mesh (66,433 nodes). However, since the primary phenomenon being studied is the air ingress into the reactor vessel, the molecular composition data is of greater importance when deciding if the solution has properly converged. Since all molecular composition data agrees, it will be assumed that no further mesh refinement is needed after 28,380 nodes.

3.4 Model Physics

This section is to explain the turbulence and physics applied to the CFD model. It also explains the reasoning for the selection of specific physics models utilized by all initial condition cases.

3.4.1 Turbulence

Due to the uncertainty inherent to CFD models, no turbulence model is collectively recognized as superior or more correct than another model. The selection of a turbulence model is based on the physics of flow and what has been established as standard practice for a specific class of problems. For the 2nd case of initial conditions, the simulation is initiated by a strong depressurization as helium flows from the 0.8 MPa vessel to the 0.101 MPa blow down tank. The ratio P_u / P_d, where P_u is the absolute upstream pressure and P_d is the absolute downstream pressure, gives the minimum pressure ratio for the initiation of choked flow in helium, which is 2.049 [32]. The pressure ratio for this system is found to be 7.92 which is well above the minimum requirement. Therefore, it can be safe to assume that the helium during depressurization is turbulent. All three initial conditions cases deal with flow after the depressurization stage. After depressurization the flow becomes stratified, where the driving force is the existing density gradients between the two fluids. Stratified flow is presumed to be comparatively slow and would theoretically have a low Reynolds number. During lock exchange, flow initial calculation indicates that the Reynolds number for helium could be around 2585 and the Reynolds number for air would be in the area of 18618. These

numbers indicate that the helium would be in the transitional flow regime while the flowing air would be turbulent. It is also important to consider the interface between the helium and air flows. At this interface it can be assumed that friction exists between the two fluids. Taking these considerations into account, it was deemed that the K-Epsilon turbulence model, a Reynolds-Average Navier-Stokes turbulence model, would be best suited for this problem. Using the K-Epsilon model also provides a good compromise between computational cost and accuracy, and model robustness [30]. Moreover, the K-Epsilon model utilizes a low Reynolds number turbulent regime which has been previously demonstrated as a high-quality model for air ingress flow [10].

The K-Epsilon model is a two equation model that uses the transport equation to solve for the flow kinetic energy, K, and its dissipation, ε. The equation blow gives the terms for k-epsilon mean flow kinetic energy [31].

$$\frac{\partial(\rho K)}{\partial t} + div(\rho K U) = div\left(-PU + 2\mu U S_{ij} - \rho U\overline{u_i' u_j'}\right) - 2\mu S_{ij}\cdot S_{ij} + \rho\overline{u_i' u_j'}\cdot S_{ij} \quad (8)$$

Rate of change of mean kinetic energy K	+	Transport of K by convection	=	Transport of K by pressure	+	Transport of K by viscous stress	+	Transport of K by Reynolds stress	-	Rate of viscous dissipation of K	-	Rate of destruction of K due to turbulence production

The governing transport equations for the k-epsilon model are [31]

$$\frac{\partial(\rho k)}{\partial t} + div(\rho k U) = div\left[\frac{\mu_t}{\sigma_k} grad k\right] + 2\mu_t S_{ij} \cdot S_{ij} - \rho\varepsilon$$
$$\frac{\partial(\rho \varepsilon)}{\partial t} + div(\rho \varepsilon U) = div\left[\frac{\mu_t}{\sigma_\varepsilon} grad \varepsilon\right] + C_{1\varepsilon}\frac{\varepsilon}{k} 2\mu_t S_{ij} \cdot S_{ij} - C_{2\varepsilon}\rho\frac{\varepsilon^2}{k} \quad (9)$$

Rate of Change of k or ε	+	Transport of k or ε by convection	=	Transport of k or ε by diffusion	+	Rate of production of k or ε	-	Rate of destruction of k or ε

No other turbulence models were used. Models such as the K-Omega, which have been shown to perform well for zero or adverse pressure gradient, did not seem applicable to this problem which involves a high pressure gradient. Other non-RANS models such as Large Eddy Simulations and Detached Eddy Simulations were not used as the problem is not concerned with eddy simulations and whose computations can be extremely expensive.

3.4.2 Discretization

The model was discretized as a transient first order, implicit, segregated flow. As a first order, upwind scheme the solution is prone to numerical diffusion. Numerical diffusion is the result of a second order spatial derivative that behaves similarly to physical diffusion. This causes errors in a discretized node to diffuse to the next node and so forth. Higher order methods tend to mitigate the effects of numerical diffusion as they use a larger number of points to calculate the spatial derivative. To evaluate the discrepancy due to numerical diffusion initial condition case 2, as it is the most severe case, was run using a second order solver. Figures 3.12 and 3.13 present the result of that

study. Using the same error calculations as in equation 9, the average difference for the molecular composition was found it be 0.0022 and 0.048 in the vessel and blow down tanks respectively. The average difference of the temperature was found to be 0.035 and 0.018 in the vessel and blow down tanks respective.

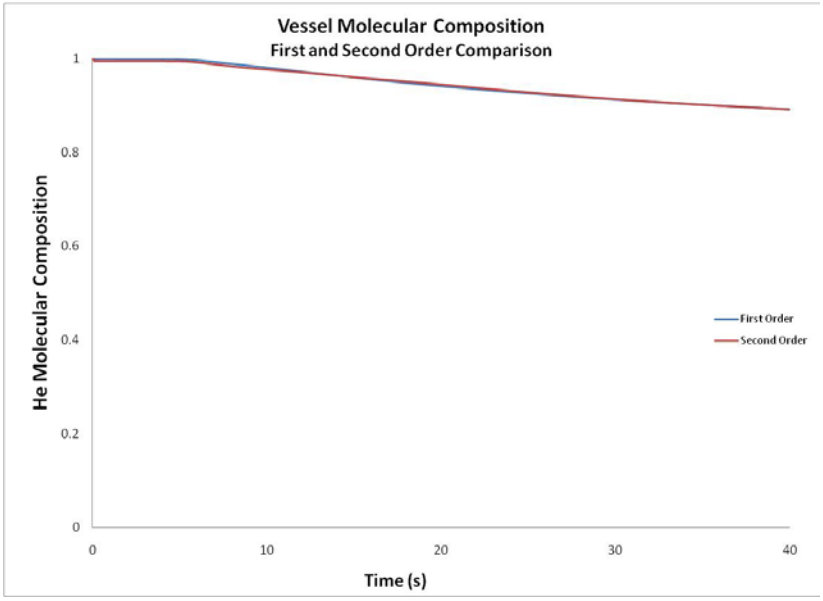

Fig 3.12: Compares the solutions for the molecular composition inside the vessel for first and second order solvers.

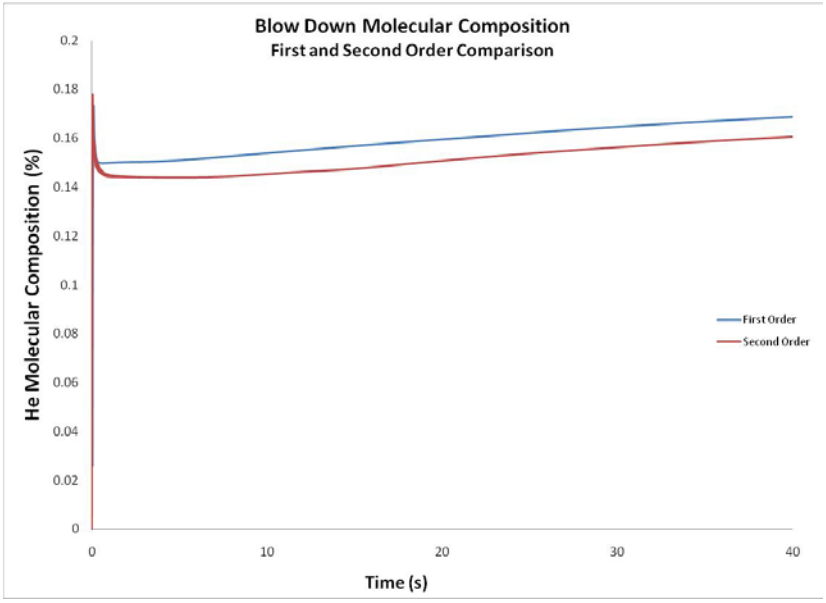

Fig 3.13: Compares the molecular composition inside the blow down tank as solved by first and second order methods.

Due to the transient nature of the problem, it was modeled implicitly. This eliminated a time dependent solution allowing for fewer needed time steps. Eliminating the time dependent solution is particularly desirable as the depressurization stage occurs very quickly. The segregated solver was selected for its lower memory requirements. However, because of the compressibility and the high velocity nature during the depressurization stage, the use of a coupled solver may result in a faster solution convergence.

3.4.3 Physics

The CFD model utilizes a multi-component gas model, which allows for the modeling of mixing gases. This allows for the simulation's two gases, helium and air, to homogenously mix in the blow down tank. The gases are modeled as ideal and as a result of the expected high velocity of the depressurization stage they are also compressible

[32]. Since the goal of this study is to observe the phenomena differences due to the depressurization during a DCC event, the gases have also been modeled as non-reacting. The nature of stratified flow and molecular diffusion necessitates the need for a gravity term to be included in the model to account for the buoyancy forces responsible for driving the air ingress flow. In STAR-CCM+ the buoyancy term for a density varying flow is given by

$$f_g = \left(\rho - \rho_{ref}\right) g \tag{10}$$

where g is the gravitational vector and ρ_{ref} is the reference density [30].

4 RESULTS

This chapter is dedicated to the CFD method results obtained for the DCC event simulation in the High Temperature Test Facility. Data collected during the CFD runs involved the monitoring of average temperature inside the vessel and blow down tank as a function of time. It also monitored the average helium molecular composition as a function of time in both tanks. Other data included visual interpretations of temperature, pressure, molecular composition, and vector flow velocities.

4.1 Event Timing

Due to the varying initial conditions, the times at which the DCC event stage initiate and finish are different. Table 4.1 shows the timing of the completion of depressurization for IC case 2. It also shows times at which exchange flow begins.

Table 4.1: Provides the times at which specific events of the DCC occur for the different initial condition cases.

IC case	Depressurization Completed	Air Enters Vessel
IC case 1	N/A	1.026 sec
IC case 2	0.235 sec	3.000 sec
IC case 3	N/A	2.38 sec

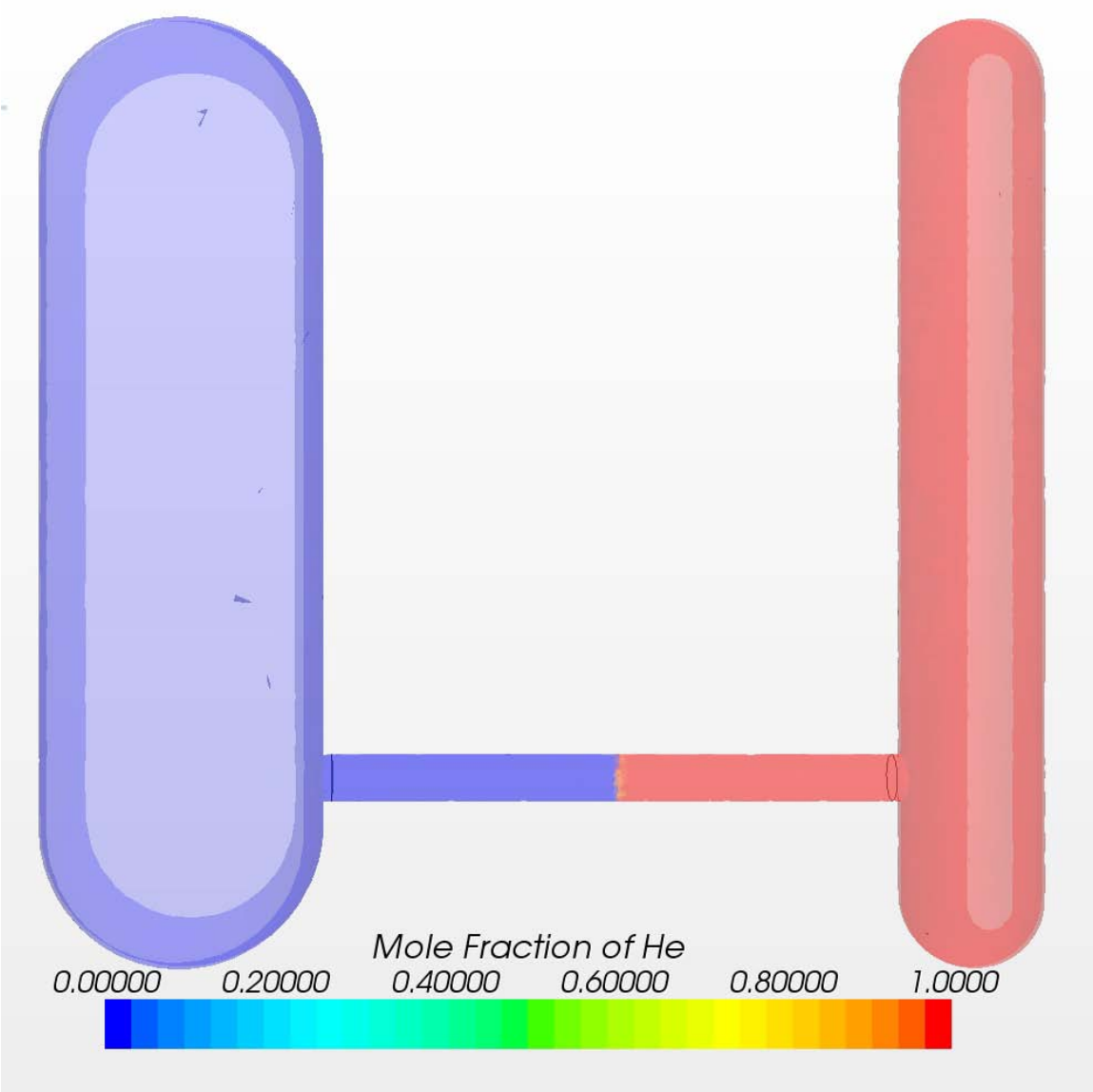

Fig 4.1: IC case 1 at time = 0.001 second.

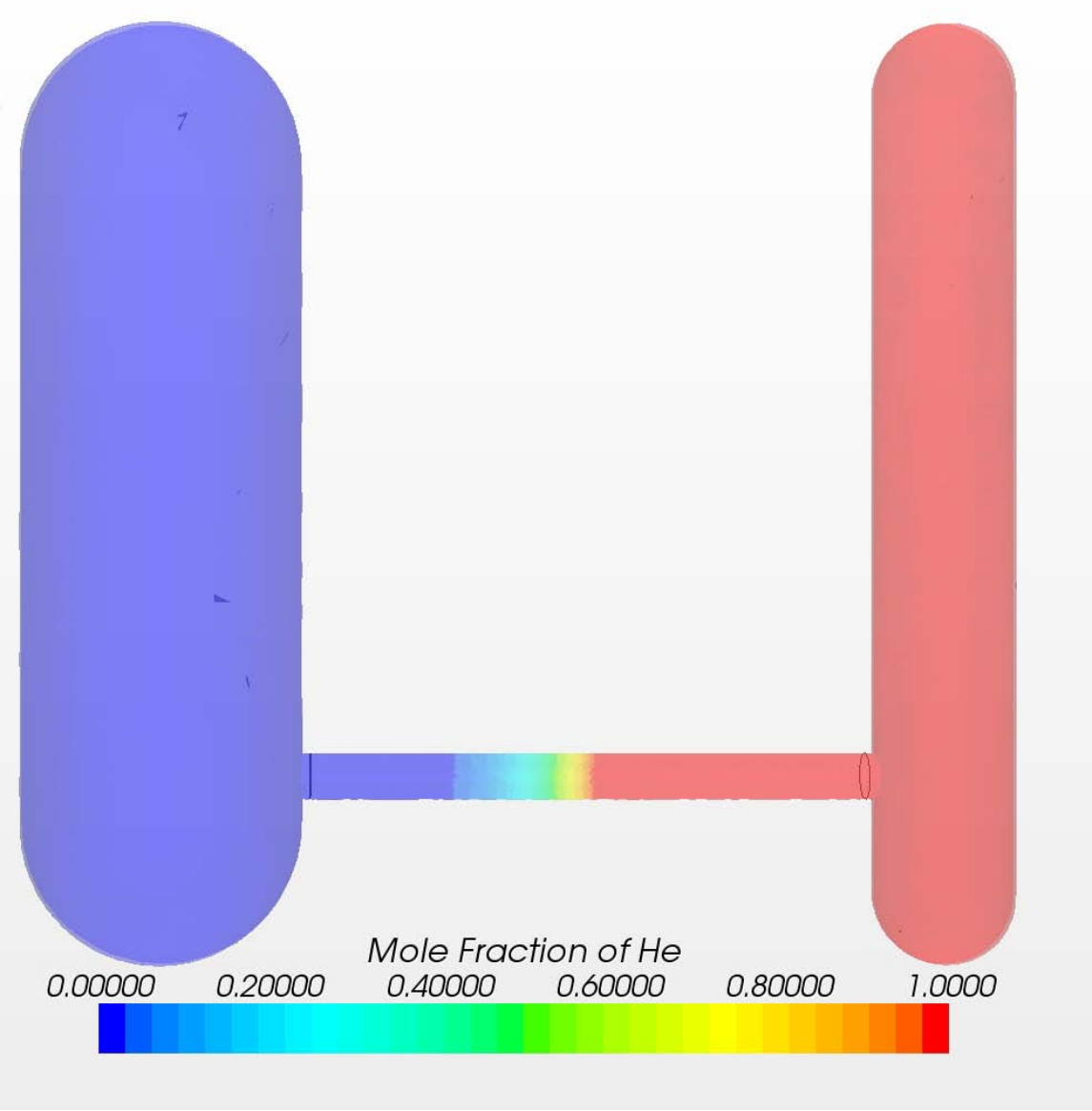

Fig 4.2: IC case 2 at time = 0.001 second

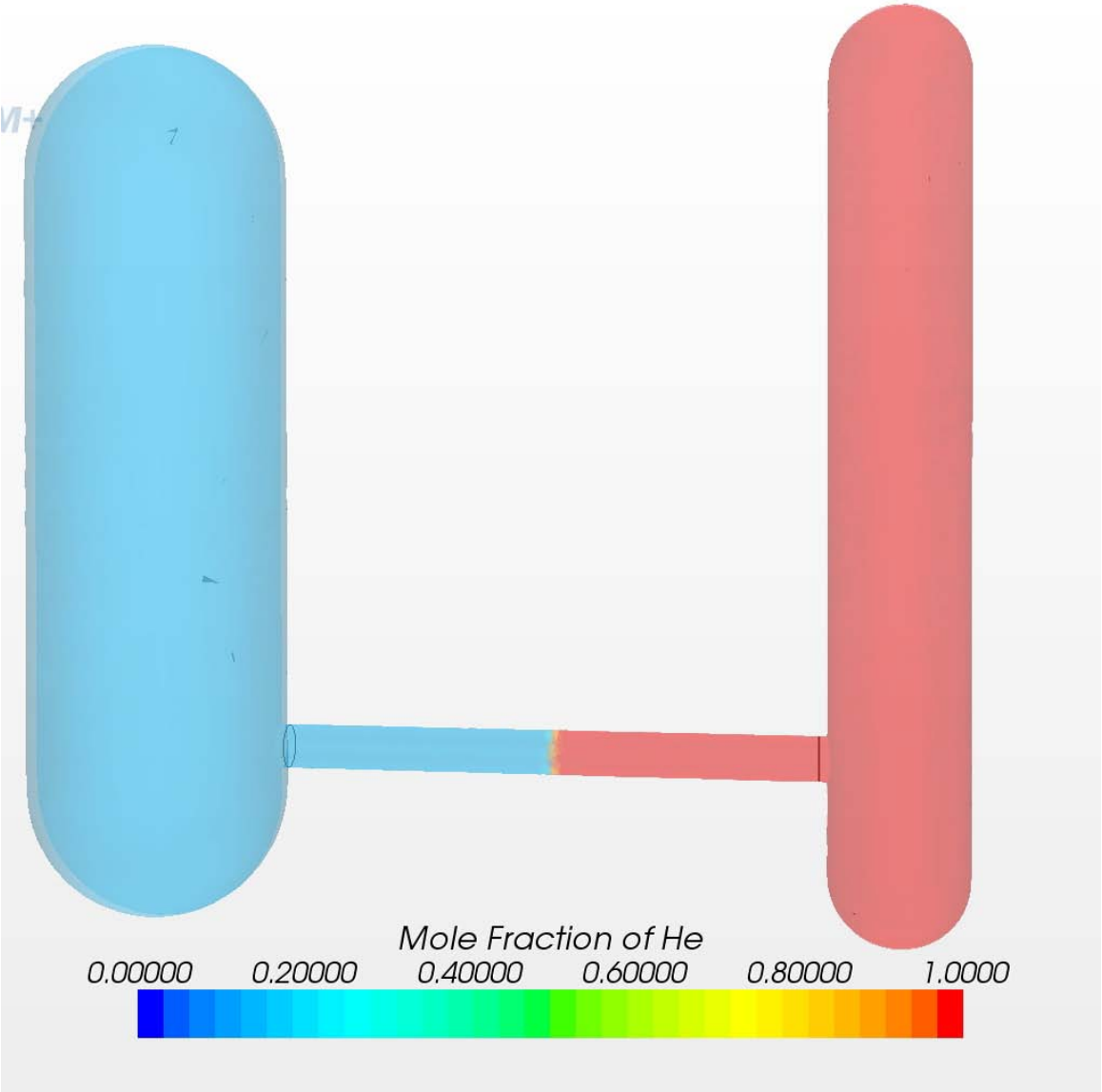

Fig 4.3: IC case 3 at time = 0.001 seconds

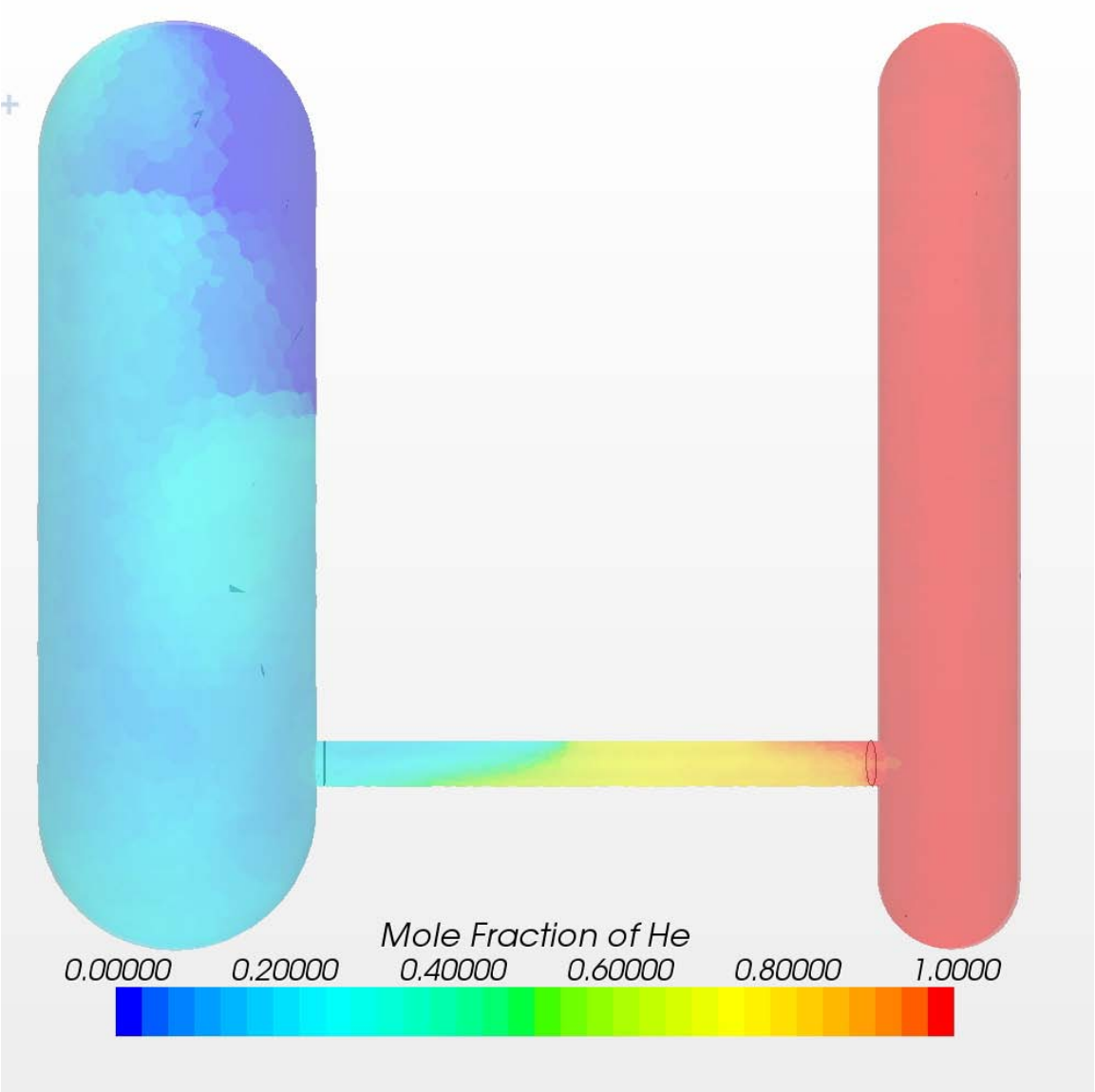

Fig 4.4: IC case 2 at time = 0.235 seconds, after system equilibrium pressure is reached.

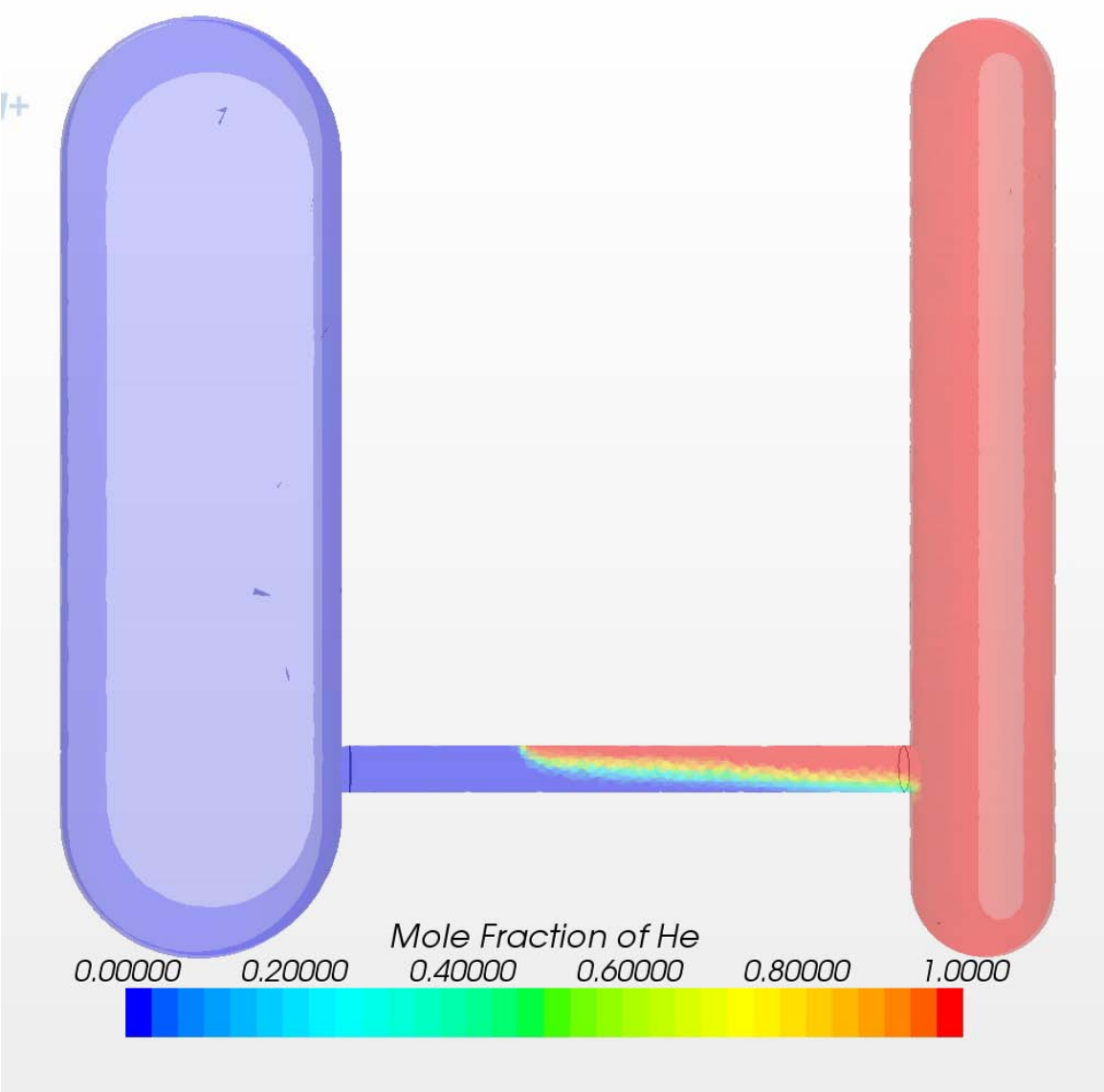

Fig 4.5: IC case 1 at time = 1.026 seconds, the onset of exchange flow.

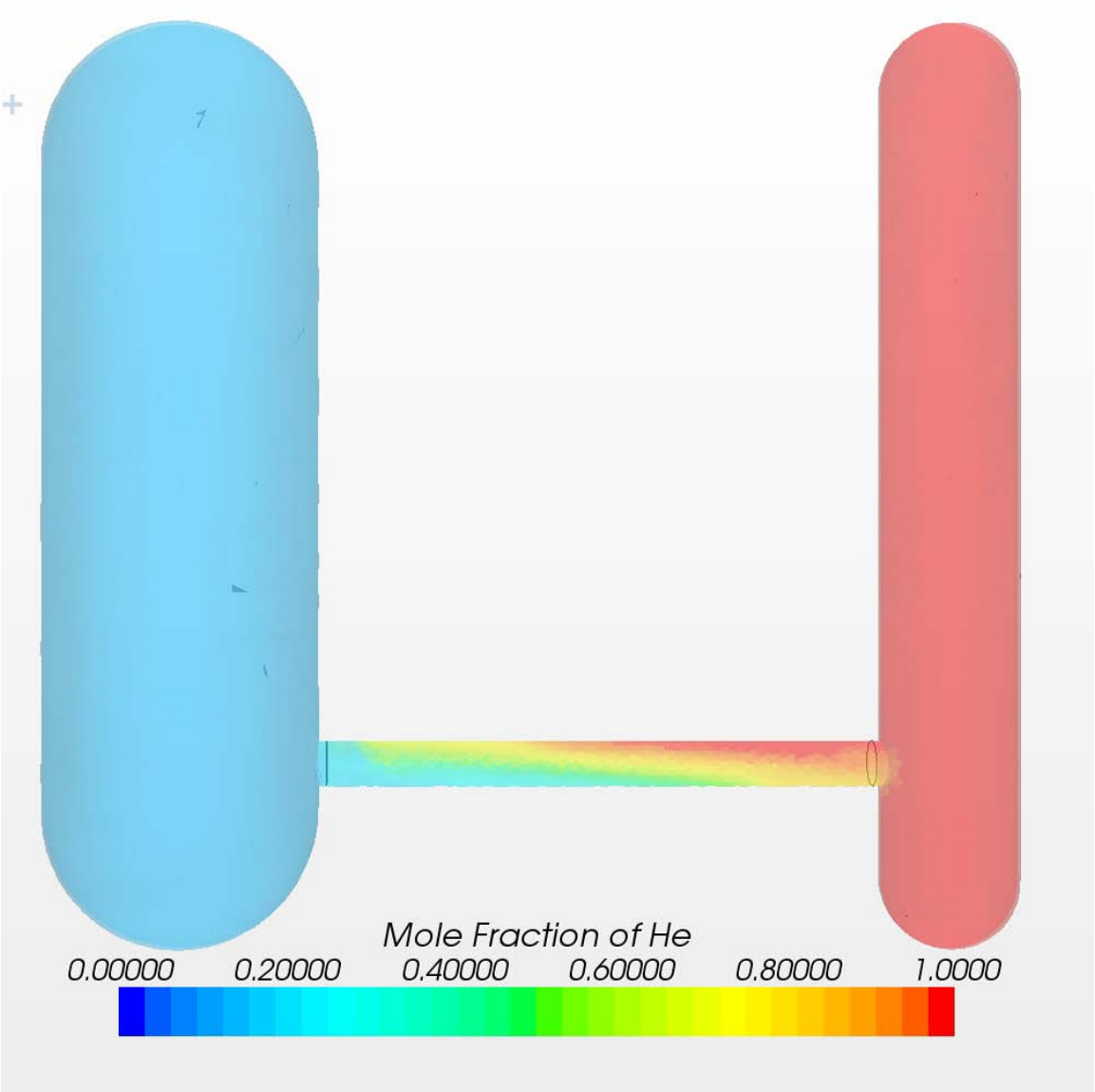

Fig 4.6: IC case 2 at time = 3.000 seconds, the onset of exchange flow.

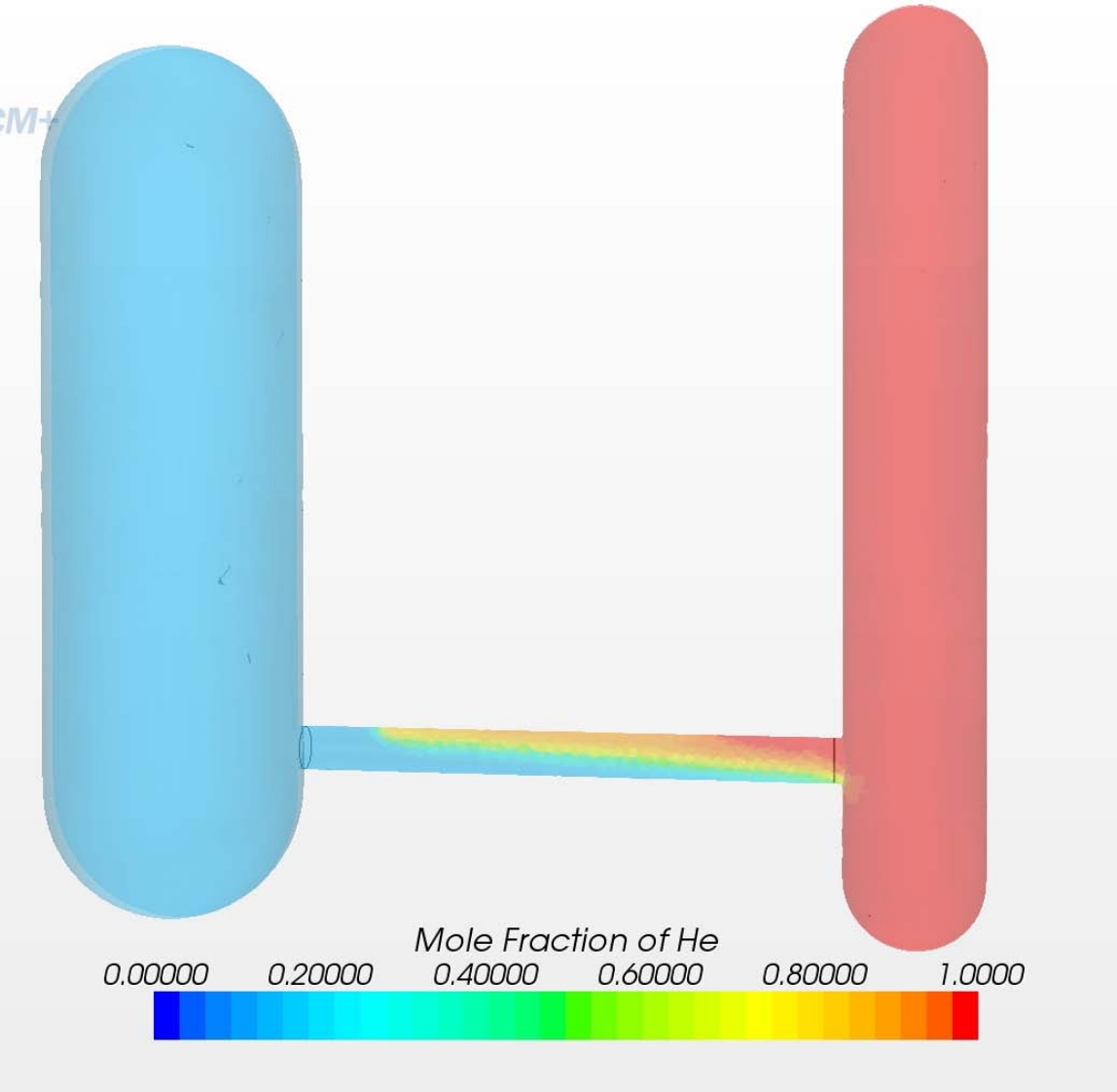

Fig 4.7: IC case 3 at time = 2.380 seconds, the onset of exchange flow.

Figures 4.1 through 4.7 show images for all three initial condition cases at different times as the DCC event stages begin to initiate. It is interesting to note that the Figure 4.6 and Figure 4.7 for IC cases 2 and 3 respectively look very similar at the onset of exchange flow.

4.2 Reactor Vessel Results

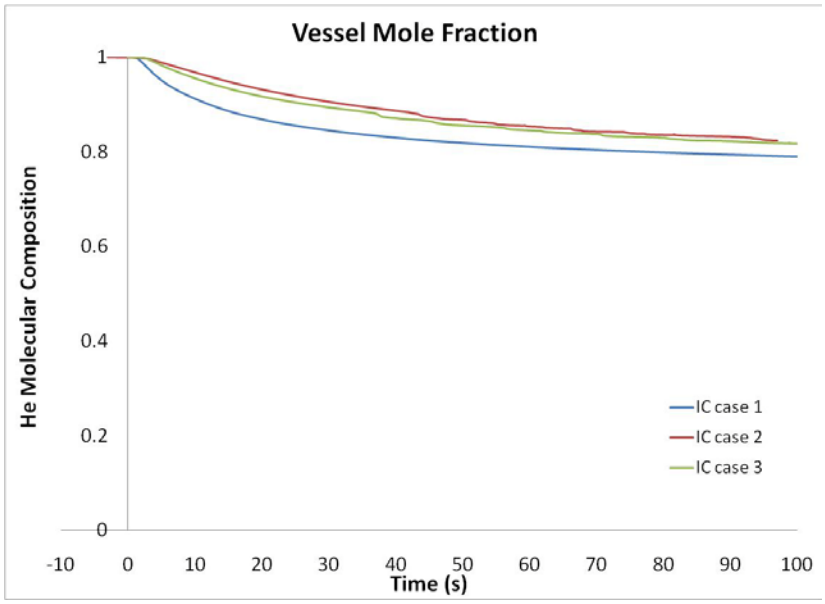

Fig 4.8: Shows the helium percentage molecular composition as a function of time in the reactor vessel of the HTTF.

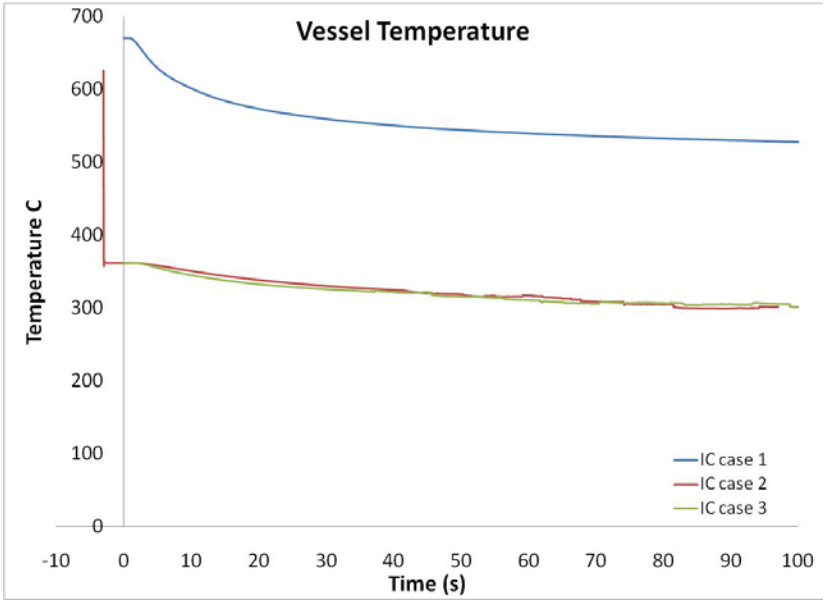

Fig 4.9: Shows the temperature as a function of time in the reactor vessel of the HTTF.

In figures 4.8 and 4.9 the red line is used to represent initial condition case 2. For comparison purposes, the time for initial condition case 2 was adjusted to make the end

of depressurization t = 0. When applying the initial condition of case 2, roughly the first 5 seconds display no change in the molecular composition of the vessel. It is during this time that the system is undergoing depressurization and then establishing exchange flow. The initiation of the decrease of the helium in the vessel indicates the established stratified flow, which ultimately brings the molecular composition down to 82 % helium. Also the temperature in the vessel experiences a sudden drop, within the first 0.1 after initiating depressurization. Before the simulation begins, the 0.8 MPa is contained in a volume of 14.4115 m^3. The system is then opened and the 0.8 MPa is allowed to depressurize into a total of volume of 18.4859 m^3. Therefore, it would be expected that the vessel would experience a quick drop in temperature.

The blue line is used to indicate the initial condition case where the entire system is set at atmospheric pressure. With the application of these initial conditions, the molecular composition of the vessel experiences a decrease in helium after the first second of simulation start up. In this case the only driving force behind fluid flow comes from the density difference existing between the helium and the air. For these initial conditions, the density of helium is 0.051547 kg/m^3 and the density of air is 1.1293 kg/m^3. As it can be seen, there is a large existing density ratio between the two fluids and this would account for lock exchange flow to initiate fairly quickly. After 100 seconds, the molecular composition of the vessel is 79 % helium. In this case the system remains at a constant volume and pressure so there is no appreciable change in vessel temperature until exchange flow is fully initiated and the air cools the hot helium in the reactor vessel.

The final case, indicated by the green line, initial conditions were setup to simulate the conditions present in the HTTF after the depressurization of a DCC event. With these conditions the reactor vessel contains 100% helium until exchange flow carries a gas mixture of 85% air and 15% helium from the blow down tank to the vessel. The density of the helium-air mixture is 0.76415 kg/m^3 and the density of the helium is 0.14992 kg/m^3, which yields a smaller density ratio; therefore, it takes slightly longer than 2 seconds before the presence of air in the vessel indicates the initiation of lock exchange flow. As the cool helium-air mixture entered, the vessel experiences a slight decrease in temperature. It is interesting to note that these initial conditions produced results very similar to the results of the initial conditions where the vessel was pressurized to 0.8 MPa.

4.3 Blow Down Tank Results

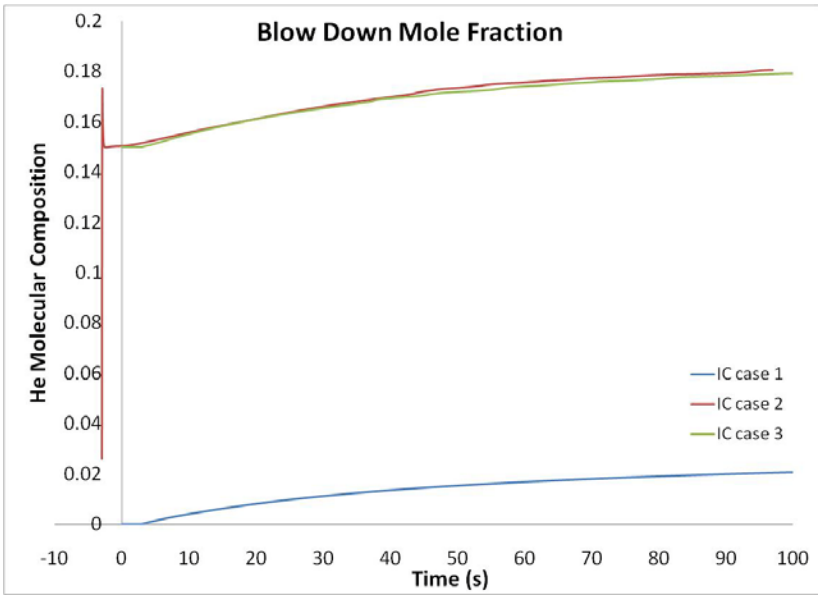

Fig 4.10: Shows the helium percentage of molecular composition as a function of time in the blow down tank of the HTTF.

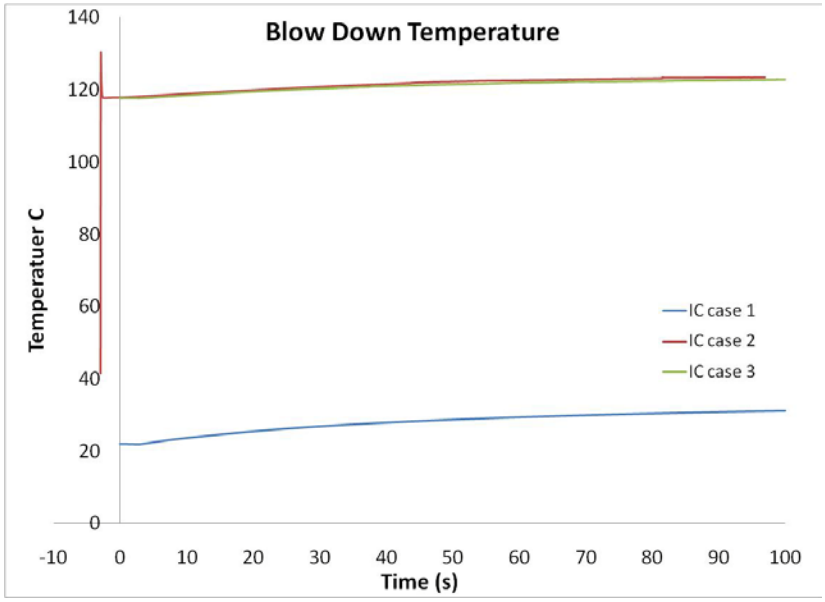

Fig 4.11: Shows the temperature as a function of time in the blow down tank of the HTTF.

As in figures 4.8 and 4.9, the red line in figures 4.10 and 4.11 is used to show the case where the initial conditions have the vessel pressurized to 0.8 MPa. During these

applied initial conditions, the blow down tank experiences a quick influx of pressurized helium. This influx causes a spike in the helium mole fraction in the blow down tank, peaking at about 17.3 % helium within the first 0.07 seconds. Due to a 'burping' effect caused by the depressurization's initial momentum, the molecular composition then drops to about 14.1 % helium and plateaus around this value for the next 4 seconds. It is at this point that helium slowly begins to enter the blow down tank through lock exchange flow resulting in an 18 % helium content in the blow down tank after 100 seconds. Similar to the molecular compositions, the temperature also experiences a very fast increase, due in part to the introduction of hot helium as well as the subsequent pressure increase, from 22 °C to a maximum of 130 °C which then experiences a quick drop to about 118 °C, after which 5 seconds pass before the initiation of lock exchange further increases the temperature to 123 °C.

The blue line indicates the initial condition case where the vessel is set to atmospheric pressure. In this simulation the helium content of the blow down tank remains at 0 % for about the first three seconds after which the buoyancy force slowly carries helium into the blow down tank until it reaches approximately 2 % helium. Similarly, the temperature experiences no sudden increase but rather increases slowly to 31 °C due to slow moving exchange flow introducing hotter helium in the blow down vessel.

The green line indicates the initial condition case where the vessel and blow down are set to equal pressure of 0.283 MPa. During this simulation, it took roughly 2.5

seconds for helium to reach the blow down tank indicating that it took about that same amount of time for exchange flow to initiate. Similarly the temperature of the blow down tank exhibits a very slow increase around the same time as lock exchange flow brings in hot helium.

5 DISCUSSION AND CONCLUSIONS

The depressurization of the High Temperature Test Facility was investigated using three different CFD simulations. The first simulation had initial conditions where the blow down tank and the reactor vessel were set to an equal pressure of 1 atmosphere and the temperature was set to 22 °C and 670 °C, respectively. Also, the blow down tank was set to be filled entirely with air and the reactor vessel was filled with helium. In the second CFD simulation, the initial conditions were set such that the blow down tank was filled with air at atmospheric pressure and a temperature of 22 °C and the vessel was filled with helium at 670 °C and a pressure of 0.8 MPa. The final simulation used initial conditions similar to what would be expected after depressurization has occurred. In this case, both tanks were set to a pressure of 0.283 MPa, the blow down tank was filled with 85 % air and 15 % helium at 118 °C while the vessel was still filled with 100 % helium at 634 °C. The following sections are dedicated to the discussion of the conclusions drawn from the CFD result.

5.1 Discussion

Once the system has reached an equilibrium pressure, it is possible to calculate the amount of air that will ingress into the vessel due to lock exchange flow. To do this the ratio between the volume of the vessel below the cross duct and the total volume of the vessel is equal to the amount of fluid that ingresses into the vessel. According to the volume of the vessel, the prescribed ratio is 0.21065 or 21.065 % . For the case where the system is set to 1 atm, the amount of air that entered the vessel was found by CFD methods to be 21.019 %. This is only a 0.22 % difference from the theoretical calculated value of 21.065%. Using the same ratio, it can be predicted that the helium-air mixture coming from the blow down tank should fill 21.065 % of the vessel. From this the percentage amount fluid that ingresses into the vessel during initial condition cases 2 and 3 can be calculated

$$\begin{aligned} VesselContents &= 0.78935He + 0.21065\left(0.85Air + 0.15He\right) \\ VesselContents &= 0.82095He + 0.1797Air \end{aligned} \tag{11}$$

This translates to an estimated value of 82.1 % of helium in the vessel. The CFD simulations for initial condition case 2 estimated 82.3% of helium to be in the vessel and 81.6% of helium in the vessel for initial condition case 3. Once again this is only 0.23 % and 0.61 % difference from the theoretical value of 82.1 % for initial condition cases 2 and 3 respectively.

5.2 Data Conclusions

Previous DCC event studies have assumed depressurization has already occurred before beginning their analysis. It was the goal of this study to observe the effects an initial depressurization would have on a CFD study of DCC events. In the case where the vessel was pressurized to 0.8 MPa, the final helium mole fraction in the vessel was 82.3 % helium making the contents of the vessel 17.7 % air. The final temperature of the vessel was 300.45 °C. In the case that sets the two tanks at atmospheric pressure, the final molecular composition in the vessel came out to be 21.0 % air and the final temperature was 527.50 °C. It is seen that the vessel contains an extra 3.3 % of air and over 200 ° C difference exist between the two models. However, when the final initial condition case 3, where the two tanks are set to 0.283 MPa and the molecular compositions mimics only the depressurized of the HTTF, the final molecular composition of the vessel is 18.4 % air and the final temperature was 301.1 °C. These results are very similar to those obtained from the simulation where the vessel was at 0.8 MPa. These results suggest that the initial starting condition that most greatly affects the air ingress is not the pressure gradient between the vessel and blow down tank but rather the density difference between the two fluids.

For initial condition case 2 the vessel pressure was set to 0.8 MPa. The data indicates that it takes approximately 4 seconds before air enters the vessel, thus indicating that after 4 seconds lock exchange flow has initiated (this includes depressurization time). In initial condition case 3 the two tanks were set to 0.283 MPa. The system took

approximately 2.5 seconds for lock exchange flow to initiate. Since these initial conditions were selected to mimic those of IC case 2 after depressurization, the density ration between the vessel and the blow down tank are equal and it can be inferred that it took approximately 1.5 seconds for IC case 2 to depressurize into the blow down tank. Initial condition case 1 set both the blow down tank and vessel at atmospheric pressure; the system took slightly longer than 1 second to initiate lock exchange flow. It is during these initial conditions that the system maintains the largest density ratio between the helium and air and results in the fastest time for exchange flow initiation. This is yet another indication that the density difference between the two fluids is the principal force driving air ingress.

Finally, the data suggest that a DCC event can be modeled without the depressurization stage provided the proper initial conditions for pressure, temperature, and molecular composition are known. This is indicated by the simulation where the applied initial conditions are those obtained after the depressurization of the system. With these initial conditions (and the already assumed depressurization), the simulation produces results almost identical to the results generated by the simulation where the vessel is allowed to depressurize. Assuming that the worst possible consequence resulting from a DCC event is the introduction of air to the graphite structure, the simulation where the initial conditions are pressure set to 1 atm, the vessel filled with helium, and the blow down tank is filled with air produces the most conservative model. This simulation contains the greatest density gradient between the two fluids and

therefore produces the faster lock exchange initiation. Due to the blow down tank filled 100 % with air, it also ingresses the most air into the vessel.

5.3 Future Work

In this problem a very simplified geometry of the high temperature test facility was used. In this instance the momentum from depressurization had no effect on the consequence of exchange flow. However, it is recommend that a more advanced geometry of a MHTGR be utilized in future studies. An advanced geometry of a MHTGR would include a vessel surrounded by a vessel cavity and a containment, as well as a lower and upper plenum support structures and flow duct inside the vessel. In the event of DCC, the vessel would depressurize into the vessel cavity. In this instance the cavity wall is closer to the break and may cause greater effects due to depressurization.

Both depressurization and exchange flow are highly dependent on the size, location, and orientation of the pressure boundary breach. It is also recommended that a study to investigate the effects of size, location, and orientation on a pressure boundary breach be conducted. Such a study may show significant differences in the amount of air ingressed into the reactor vessel and the rate at which it occurs.

This problem also utilizes isothermal temperatures. After the simulation is initiated there is no heat added to the system. It is suggested that to simulate more accurately a reactor's loss of coolant accident decay heat would need to be included. Decay heat would be an important factor as it would maintain a higher temperature in the

vessel which in turn would maintain a greater density gradient between the fluids possibly allowing more air to ingress into the vessel.

BIBLIOGRAPHY

1. Kadak, A.C., Zhai, T., 2004, "Air Ingress Benchmarking with Computational Fluid Dynamics Analysis," 2nd International Topical Meeting on High Temperature Reactor Technology, Beijing, China.

2. Wolters, J., Breitback, G., Moormann, R., "Air and Water Ingress Accidents in a HTR-Modul of Side-by-Side Concept," Jülich Research Center, Juelich, Germany.

3. Hishida, M., Fumizawa, M., Takeda, T., Ogawa, M., Tekenaka, S., 1993, "Researches on Air Ingress Accidents of the HTTR," Nuclear Engineering and Design 144, pp. 317-325.

4. Hishida, M., Takeda, T., 1991, "Study on Air Ingress During an Early Stage of a Primary-Pipe Rupture Accident of a High-Temperature Gas-Cooled Reactor," Nuclear Engineering and Design 126, pp. 175-187.

5. Ball, Syd, 2006, "Sensitivity Studies of Modular High-Temperature Gas-Cooled Reactor Postulated Accidents," Nuclear Engineering and Design 236, pp. 454-462.

6. Haque, H., 2008, "Consequences of Delayed Air Ingress Following a Depressurization Accident in a High Temperature Reactor," Nuclear Engineering and Design 238, pp. 3041-3046.

7. Reyes, J., Woods, B., Marshall, T., May, 2008, "Developing Core Flow Analysis Methods for the VHTR and GFR Designs," NUC/IUC Symposium, Idaho Falls, Idaho.

8. Reyes, J.N., Groome, J., Woods, B., Jackson, B., Marshal, T., 2010, "Scaling Analysis for the High Temperature Gas Reactor Test Section (GRTS)," Nuclear Engineering and Desing 240, pp. 397-404.

9. Oh, Chang, Kim, E.S., Schultz, R., Petti, D., Liou, C.P., 2008, "Implications of Air Ingress Induced by Density-Difference Driven Stratified Flow," Idaho National Laboratory.

10. Oh, Chang, Kim, E.S., Schultz, R., Petti, D., Kang, H., 2009, "Computational Fluid Dynamics Analyses on Very High Temperature Reactor Air Ingress," Idaho National Laboratory.

11. Oh, Chang, Kim, E.S., 2010, "Air Ingress Analysis: Computation Fluid Dynamic Models," Idaho National Laboratory.

12. Oh, Chang, Kim, E.S., 2011, “Air-Ingress Analysis: Part 1. Theoretical Approach,” Nuclear Engineering and Design 241, pp. 203-212.

13. Oh, Chang, Kang, H.S., Kim, E.S., 2011, “Air-Ingress Analysis: Part2 – Computational Fluid Dynamic Models,” Nuclear Engineering and Design 241, pp. 213-225.

14. Oh, Chang, Kim, E.S., 2010, “Validations of CFD Code for Density-Gradient Driven Air Ingress Stratified Flow,” Idaho National Laboratory.

15. Duncan, J.B., H.L. Toor, 1962, “An Experimental Study of Three Component Gas Diffusion,” A.I.Ch.E Journal 8, pp. 1-38.

16. Wilkinson, B.L., 1983, “Motion of Air Caviies in Lob Horizontal Ducts,” J. Fluid Mech. 118, pp. 109-122.

17. Shin, J.O., S.B. Dalziel, P.F. Linden, 2004, “Gravity Currents Produced by Lock Exchange,” J. Fluid Mech. 521, pp. 1-34.

18. Huppert, H.E., J.E. Simpson, 1980, “The Slumping of Gravity Currents,” J. Fluid Mech. 99, pp. 785-789.

19. Huppert, H.E., 1982, “The propagation of Two-Dimensional and Axisymmetric Viscous Gravity Currents Over a Rigid Horizontal Surrace,” J. Fluid Mech. 121, pp. 43-58.

20. Britter, R.E., J.E. Simpson, 1981, “A Not on the Struction fo the head of an intrusive Gravity Current,” J. Fluid Mech. 112, pp. 459-466.

21. Benjamin, T.B., 1968, “Gravity Currents and Related Phenomena,” J. Fluid Mech. 31 part 2, pp. 209-243.

22. Klemp, J.B., R. Rotunno, W.C. Skamarok, 1994, “On the Dynamics of Gravity Currents in a Channel,” J. Fluid Mech. 264, pp. 169-198.

23. Étienne, J., E.J. Hopfinger, P. Saramito, 2005, “Numerical Simulations of high Density Ratio Lock-Exchange Flows,” Physics of Fluids 17.

24. Henry, C.E., R.E. Henry, R.T. Lahey, S.G. Bankoff, 1993, “Bouyantly-Driven Two-Phase Countercurrent Flow in Liquid Discharge from a Vessel with an Unvented Gas Space,” Nuclear Engineering and Design 141, pp. 237-248.

25. Didden, N., T. Maxworthy, 1982, “The Viscous Spreading of Plane and Axisymmetryic Gravity Current,” J. Fluid Mech. 121, pp. 27-42.

26. MacDonald, P.E., et al., *NGNP Preliminary Point Design—Results of the Initial Neutronics and Thermal-Hydraulic Assessments,* INEEL/EXT-77-00870 Rev. 1, September 2003.

27. Vallée, C., D. Lucas, M. Beyer, H. Pietruske, P. Schütz, H. Carl, 2009, "Experimental CFD Grade Data for Stratified Two-Phase Flow," Nuclear Engineering and Design

28. Martín-Valdepeñas, J.M., M.A. Jiménez, F. Martín-Fuertes, J.A. Fernández, 2006, "Improvements in a CFD Code for Analysis of Hydrogen Behavior within Containments," Nuclear Engineering and Desing, 237

29. Simoneəu, J., J.Champigny, B. Mays, L. Lommers, 2007, "Three-Dimensional Simulation of the Coupled Convective, Conductive and Radiative Heat Transfer During Decay Heat Removal in an HTR," Nuclear Engineering and Design, 237, pp. 1923-1937.

30. STAR-CCM + User Guide

31. Versteeg, H., W. Malalasekra, An Introduction to Computational Fluid Dynamics, 2nd edition,

32. Fox, R.W., A. Mcdonald, P. Pritchard, Introduction to Fluid Mechanics, 6th edition.

33. Ferziger, J.H., M. Perić, Computational Methods for Fluid Dynamics, 3rd edition.